LBL-16262 c.2

Lawrence Berkeley Laboratory

UNIVERSITY OF CALIFORNIA

RECEIVED
LAWRENCE
BERKELEY LABORATORY

MAR 14 1984

LIBRARY AND
DOCUMENTS SECTION

Materials & Molecular Research Division

INFLUENCE OF VISCOUS ENVIRONMENTS ON FATIGUE CRACK PROPAGATION IN A LOWER STRENGTH STEEL

J.-L. Tzou
(M.S. Thesis)

June 1983

TWO-WEEK LOAN COPY

This is a Library Circulating Copy which may be borrowed for two weeks. For a personal retention copy, call Tech. Info. Division, Ext. 6782.

LBL-16262 c.2

Prepared for the U.S. Department of Energy under Contract DE-AC03-76SF00098

DISCLAIMER

This document was prepared as an account of work sponsored by the United States Government. While this document is believed to contain correct information, neither the United States Government nor any agency thereof, nor the Regents of the University of California, nor any of their employees, makes any warranty, express or implied, or assumes any legal responsibility for the accuracy, completeness, or usefulness of any information, apparatus, product, or process disclosed, or represents that its use would not infringe privately owned rights. Reference herein to any specific commercial product, process, or service by its trade name, trademark, manufacturer, or otherwise, does not necessarily constitute or imply its endorsement, recommendation, or favoring by the United States Government or any agency thereof, or the Regents of the University of California. The views and opinions of authors expressed herein do not necessarily state or reflect those of the United States Government or any agency thereof or the Regents of the University of California.

LBL-16262

INFLUENCE OF VISCOUS ENVIRONMENTS ON FATIGUE CRACK PROPAGATION IN A LOWER STRENGTH STEEL

Jye-Len Tzou

Materials and Molecular Research Division, Lawrence Berkeley Laboratory,
and Department of Materials Science and Mineral Engineering,
University of California, Berkeley, CA 94720

June 1983

M.S. Thesis

INFLUENCE OF VISCOUS ENVIRONMENTS ON FATIGUE CRACK PROPAGATION IN A LOWER STRENGTH STEEL

Jye-Len Tzou

Materials and Molecular Research Division, Lawrence Berkeley Laboratory,
and Department of Materials Science and Mineral Engineering,
University of California, Berkeley, CA 94720

ABSTRACT

The effect of dehumidified silicone and paraffin oils with viscosities from 5 to 60,000 centistokes (cS) on fatigue crack propagation in a lower strength 2¼Cr-1Mo pressure vessel steel (ASTM A542 Class 3) has been studied at both near-threshold ($\leq 10^{-6}$ mm/cycle) and higher ($\sim 10^{-6}$ to 10^{-3} mm/cycle) growth rates. It is found that, at low load ratios, crack growth rates in oils are lower than in moist air and dry hydrogen and increase with increasing oil viscosity in higher growth rate region. However, at near-threshold levels, crack growth rates in oils are considerably higher than in moist air and are not affected by the viscosity of oil. At high load ratios, although crack propagation in oils is slower in higher growth rate region and unchanged at near-threshold levels when compared to that in moist air, no effect of oil viscosity can be observed.

Such observations are discussed and quantitatively analyzed in terms of three mutually competitive mechanisms specific to dry viscous environments, namely suppression of moisture-induced hydrogen embrittlement and/or metal dissolution, minimization of oxide-induced crack closure and hydrodynamic wedging effects of the viscous fluid within the crack.

NOTICE OF CORRECTIONS

The development and the quantitative analysis of the viscous fluid-induced crack closure model in this thesis have recently been improved using numerical analysis methods. The major aspects of the improved modelling work which will be published in LBL Report No. 16028, October 1983, can be summarized as follows:

Under specific testing conditions, the magnitude of the instantaneous environmental fluid penetration distance into a fatigue crack as a function of time (or number of fatigue cycles) and the corresponding hydrodynamic pressure-induced stress intensity increment (and hence the real stress intensity range, ΔK, responsible for the crack growth) can be continuously predicted without using any adjustable parameters. Generally speaking, any required quantitative information and predictions about the fatigue crack growth in viscous fluid environments can be obtained from the simultaneous solutions of the integrated form of the equations listed in Table IX.

As far as the current study is concerned, the improved model generated the basically similar predictions about the viscous fluid-induced crack closure behavior in fatigue crack growth as the old one did. However, the improved analysis can yield quantitative predictions on the rate of oil penetration as a function of crack propagation rate such that the distinction between the use of partial or full penetration models becomes clearcut.

INFLUENCE OF VISCOUS ENVIRONMENTS ON FATIGUE

CRACK PROPAGATION IN A LOWER STRENGTH STEEL

TABLE OF CONTENTS

	Page
ACKNOWLEDGEMENTS	iii
NOMENCLATURE	iv
1. INTRODUCTION	1
1.1 Conceptual Background	1
1.2 Scope of Present Study	4
2. EXPERIMENTAL PROCEDURE	5
2.1 Preparation of Material and Specimens	5
2.2 Preparation of Environmental Oils	5
2.3 Fatigue Crack Growth Test Procedures	6
2.4 Analysis of Fracture Surfaces	8
2.4.1 Fractography/Scanning Electron Microscopy (SEM)	8
2.4.2 Auger Electron Spectroscopy (AES)	8
3. RESULTS	9
3.1 Fatigue Crack Propagation	9
3.1.1 General Observations	9
3.1.2 Effects of Oil Viscosity and Chemistry	10
3.2 Analysis of Fracture Surfaces	11
3.2.1 Auger Electron Spectroscopy	11
3.2.2 Fractography	12

Page

4. DISCUSSION 13

4.1 Viscous Fluid-Induced Protective Effects 13

4.2 Viscous Fluid-Induced Crack Closure 17

4.2.1 Effect of a Hydrodynamic Wedge 17

4.2.2 Estimation of the Closure Stress Intensity (K^{w}_{cl}) Due to Hydrodynamic Wedge Actions 22

4.3 Effect of Load Ratio (or Mean Stress) 29

5. CONCLUSIONS 31

REFERENCES 34

APPENDIX 42

A. Determination of the Resultant Hydrodynamic Force within a Closing Fatigue Crack Partially Penetrated by a Viscous Fluid 42

B. Determination of the Resultant Hydrodynamic Force within a Closing Fatigue Crack Fully Penetrated by a Viscous Fluid 44

TABLES 46

FIGURES 53

ACKNOWLEDGEMENTS

The author would like to extend his appreciation and gratitude to Professor Robert O. Ritchie for his support, guidance and encouragement throughout this investigation and for providing a stimulating ambient to work in.

Special thanks go to Dr. Subra Suresh for his initial orientation to all the experimental and analytical techniques employed and the subsequent valuable discussions and suggestions during the entire course of this work. The author also thanks all the other member in Professor Ritchie's research group for their helpful comments and suggestions on this work and their friendship.

Thanks are also due to the technical personnel of the Materials and Molecular Research Division, Lawrence Berkeley Laboratory, for their help in fatigue tests, Auger electron spectroscopy and scanning electron microscopy.

The author would like to dedicate this work to his parents and girlfriend, Theresa, for their distant support, encouragement and love, which have kept him always at a very high momentum.

Finally, the author would like to express his gratitude to Madeleine Penton for typing this manuscript and to Professors J. W. Morris, Jr., and A. G. Evans for critical reading of this manuscript and comments towards making this a better study.

This study was supported by the Director, Office of Energy Research, Office of Basic Energy Sciences, Material Science Division of the U.S. Department of Energy, under Contract No. DE-AC03-76SF0009.

NOMENCLATURE

a	crack length
a_o	initial crack length or notch depth of CT specimens
b	ligament of cracked specimen (W-a)
B	specimen thickness
c	the distance between the centroid of the hydrodynamic pressure distribution and the loading line of CT specimen
d	penetration distance of fluid into an arbitrary edge crack
d_{eff}	effective penetration distance of fluid into a crack in *CT* specimen
da/dN	fatigue crack growth rate per cycle
$d\theta/dt$	angular closing velocity of crack walls
D	excess oxide thickness measured on fracture surface
E	elastic modulus
f	cyclic frequency
F_f^e	resultant hydrodynamic force (per unit thickness) at minimum load during fatigue cycle due to *full* fluid penetration into an *edge* crack
F_p^e	resultant hydrodynamic force (per unit thickness) at minimum load during fatigue cycle due to *partial* fluid penetration into an *edge* crack
F_p^c	resultant hydrodynamic force (per unit thickness) at minimum load during fatigue cycle due to *partial* fluid penetration into a crack in *CT* specimen
h	crack mouth opening displacement (CMOD)
h_{max}	maximum crack mouth opening displacement
h_{min}	minimum crack mouth opening displacement
H	average crack opening width
H_{max}	maximum average crack opening width
H_{min}	minimum average crack opening width

$\bar{H}$	mean of the maximum and the minimum average crack opening widths ($\frac{1}{2}(H_{max} + H_{min})$)
K	linear elastic stress intensity factor
K_c	stress intensity factors at final failure (fracture toughness)
K_{cl}	stress intensity to cause closure of the crack
K_{cl}^w	closure stress intensity due to hydrodynamic wedge actions
K_f^e	stress intensity increment at minimum load due to *full* fluid penetration into an *edge* crack
K_f^c	stress intensity increment at minimum load due to *full* penetration into a crack in *CT* specimen
K_{max}	maximum stress intensity during fatigue cycle
K_{min}	minimum stress intensity during fatigue cycle
K_p	stress intensity increment at minimum load during fatigue cycle due to hydrodynamic wedge actions in the crack
K_p^e	stress intensity increment at minimum load during fatigue cycle due to hydrodynamic wedge actions caused by the *partial* fluid penetration into an *edge* crack
K_p^c	stress intensity increment at minimum load during fatigue cycle due to hydrodynamic wedge actions caused by the *partial* fluid penetration into a crack in *CT* specimen
ℓ	half the distance between location of peak oxide layer and crack tip
$p(x)$	pressure as a function of distance x (or pressure distribution)
p_f^c	resultant hydrodynamic pressure at minimum load during fatigue cycle due to *full* fluid penetration into a crack in *CT* specimen
p_f^e	resultant hydrodynamic pressure at minimum load during fatigue cycle due to *full* fluid penetration into an *edge* crack
Q, Q', Q''	geometric factor dependent upon the crack geometry and the extent of fluid penetration into the crack
r	rotational factor determining the location of the apparent plastic hinge along crack line in the specimen ligament b
R	load ratio (K_{min}/K_{max})
t	time

v	approaching velocity of fatigue crack walls during unloading half cycle
W	width of CT specimen
Y	monotonic yield strength
ΔK	stress intensity range ($K_{max} - K_{min}$)
ΔK_{eff}	effective stress intensity range taking into account crack closure ($K_{max} - K_{cl}$)
ΔK_o	threshold stress intensity range for no crack growth
α	the crack length-to-width ratio
β	wetting angle
γ_L	surface tension of fluid
δ	crack tip opening displacement (CTOD)
δ_{max}	maximum crack tip opening displacement
δ_{min}	minimum crack tip opening displacement
ε	ratio of the fluid penetration distance (d) to the crack length (a) in an *edge* crack (= d/a)
η	kinematic viscosity
η_o	initial kinematic viscosity
θ	angle formed by crack walls
ν	Poisson's ratio
ρ	density of fluid
τ,ϕ	ratio of the distance between the centroid of the hydrodynamic pressure distribution and notch root in CT specimen to the crack length
ψ	viscosity-pressure coefficient

1. INTRODUCTION

1.1 CONCEPTUAL BACKGROUND

It is well known that fatigue crack propagation behavior of many engineering materials are sensitive to mechanical, microstructural, and environmental variables, such as load ratio or mean stress (characterized by $R = K_{min}/K_{max}$), frequency, stress history, crack geometry; grain size, grain boundary composition, and yield strength of the materials; temperature, pressure, constituents of the environments, and so on [1]. Since these variables are strongly interrelated, every combination may generate different crack growth behavior in different mechanical situations. The various mechanisms associated with fatigue crack propagation behavior are summarized in Figure 1 [1] where the variation of the crack growth rate, log(da/dN) with stress intensity range, log(ΔK) is shown. This figure represents behavior from extremely low growth rates (less than 10^{-6} mm/cycle) approaching a so-called threshold stress intensity range ΔK_o, below which cracks remain dormant or grow at experimentally undetectable rates [1], to higher growth rates. It is evident that the role of environment in influencing fatigue crack growth behavior is most predominant in the near-threshold and mid-growth-rate regions (regimes A and B in Fig. 1) which are generally the regimes of greatest engineering interest at present.

Although many studies have focused on the influence of environments on fatigue properties of engineering materials over the last few decades, most attention has been drawn to merely a comparison of fatigue crack initiation and propagation behavior in various gaseous and aqueous environments. However, it has been recognized that the fatigue resistance

of cyclically-stressed components can be markedly affected by the presence of supposedly non-corrosive liquid environments. For example, a number of investigators [5-8] have found that the Stage II (or regime B) fatigue crack growth in both ferrous [4,6,7] and non-ferrous [5,8] alloys were slower in several kinds of non-corrosive fluids, such as mineral oils [4-7], silicone oils [6,7], etc., compared to those in air. Many studies on rolling contact fatigue behavior of high strength bearing steels in lubricant fluids [7,9-12] also indicated that the presence of water in the lubricants could largely accelerate the pitting failure of bearing balls and cause significant reductions in surface fatigue life. Such effects were attributed to conventional corrosion processes, such as hydrogen embrittlement. Moreover, recent work by Vosikovsky and co-workers [13,14] on fatigue crack growth in X65 pipeline steel tested in crude oil environments also showed that Stage II crack growth rates could be increased by 3 to 20 times compared to air as the concentration of H_2S in the oil increased from $\sim$1 ppm to saturation level ($\sim$4700 ppm). It is thus believed that the improvement in fatigue life or retardation of Stage II fatigue crack growth rates in non-corrosive fluids is mainly due to the exclusion of moisture or other corrosive species from the crack tip region and the suppression of the conventional corrosion fatigue processes.

In addition to the protective actions of viscous fluids, the role of viscosity has received much attention. In numerous investigations, fatigue lives of ball or roller bearings have been reported to increase [15-22], decrease [19] or be unchanged [19,23,24] with the increase of viscosity of the fluids. Furthermore, Endo and co-workers [5,6] found that fatigue crack propagation rates at constant stress amplitude and

constant frequency in two non-ferrous alloys [5] and a medium carbon steel [6] decreased with increase in viscosity of mineral and polymeric silicone oils. Although most of the above-mentioned results have apparently shown a general trend of increased fatigue life (or decreased fatigue crack growth rates) with increasing fluid viscosity, no satisfactory explanations have been made for the reported observations.

With regard to the effect of viscosity, it was suggested by Way [25] that the fluid penetration into cracks could act as a wedge and caused the cracks to propagate during load reversals. It was also pointed out that less viscous lubricating fluids reduced fatigue life because they could enter cracks more easily, hence accelerating fatigue crack propagation. Subsequent researchers [5,6,18-20,22,23] also explained their similar fatigue results based on this hydraulic wedge mechanism, among them Endo et al. [5,6] reported that the hydrodynamic oil pressure within a closing fatigue crack due to the penetration of oil filling the crack could reduce the stress amplitude actually experienced at the crack tip and hence lower crack growth rates.

Recently the phenomena of fatigue crack closure, including plasticity-induced crack closure [26,27], oxide-induced crack closure [28-34], and surface roughness-induced crack closure [35-40], have been well recognized and successfully used to explain many aspects of fatigue crack propagation behavior in near-threshold and higher-growth-rate regions, such as load ratio, environmental, and microstructural effects [41]. It results in a reduction of the nominal driving force ($\Delta K = K_{max} - K_{min}$) for crack extension due to the premature contact of the crack surfaces at positive loads during the unloading part of a cycle.

Based on the concept of crack closure, it is thought that the aforementioned hydrodynamic wedge mechanism due to the fluid confined within the fatigue crack can induce crack closure or a mechanism equivalent to that. Thus the hypothesis proposed by Way [25] that the fluid within cracks could accelerate crack growth is questionable from crack closure viewpoints unless the fluid pressure exceeds the maximum applied load. Since cracks are usually small enough to be treated as capillaries, the extent of the penetration of fluids into the cracks will be closely related to the capillary action [5,22,42]. However, this factor which may greatly influence the fatigue crack propagation behavior in non-corrosive viscous environments has been rarely considered in previous work in viscous environments.

1.2 SCOPE OF PRESENT STUDY

It is apparent from the above discussion that the effect of non-corrosive viscous environments on fatigue crack propagation behavior, especially in near-threshold region (regime A), is not clearly understood. The previously proposed hydrodynamic wedge mechanisms [5,6] cannot satisfactorily explain the observations of increased or unchanged fatigue life with increasing fluid viscosity. Accordingly, the objective of the present study is to examine mechanistically the effect of dehumidified silicone and paraffin oils of viscosities ranging from 5 to 60,000 cS on fatigue crack growth behavior from near-threshold to higher-growth-rate regions in a lower strength low alloy steel. The intent is to develop mechanisms and models to explain and analyze quantitatively the precise role of the viscous environments in influencing crack growth behavior with a combined fracture mechanics, hydrodynamics, and surface chemistry approach.

2. EXPERIMENTAL PROCEDURES

2.1 PREPARATION OF MATERIAL AND SPECIMENS

The steel used in this investigation was a lower strength 2¼Cr-1Mo pressure vessel steel, namely ASTM A542 Class 3 (hereafter referred to as SA542-3). A thick section of this steel (Lukens heat no. 3707) was obtained with a size of approximately 140 mm x 300 mm x 175 mm from Westinghouse Research and Development Center. The chemical composition, as-received heat treatment, and the ambient temperature mechanical properties of this steel are listed in Tables I, II and III respectively. The microstructure of SA542-3 was fully bainitic with less than 3% polygonal ferrite at plate mid-thickness, as shown in Figure 2.

ASTM standard 1-T compact tension C(T) specimens with a 12.7 mm (½ inch) thickness (Fig. 3) were machined in the T-L orientation, i.e., cracks propagate in the rolling direction (Fig. 4), between quarter and mid-thickness section of the plates. The thickness was chosen such that in subsequent tests plane strain conditions were maintained, based on the criterion that cyclic plastic zone sizes did not exceed 1/15 of test-piece thickness.

2.2 PREPARATION OF ENVIRONMENTAL OILS

Silicone and paraffin oils, each of chemical similarity but with a series of viscosity levels, were used as environments in the fatigue tests of current research program.

Silicone oils (Dimethyl Siloxane Polymer or Dimethyl Polysiloxane) with kinematic viscosities ranging from 5 to 60,000 centistokes were obtained from Dow Corning Corporation, Midland, Michigan.

Paraffin oil, a mixture of saturated aliphatic and naphthentic hydrocarbons containing 28-36 carbon atoms [44], was produced by Fisher Scientific Company, Fair Lawn, New Jersey. The viscosity of paraffin oils depends basically on the number of carbon atoms contained in the hydrocarbon constituents. Species with kinematic viscosities of 25 and 75 centistokes were chosen. The major physical properties of silicone and paraffin oils are listed in Table IV.

2.3 FATIGUE CRACK GROWTH TEST PROCEDURES

Fatigue crack propagation experiments were performed on a 98 kN, electro-servo-hydraulic MTS machine operating under load control at room temperature ($\sim$ 21°C) at a cyclic frequency of 50 Hz. The applied load was sinusoidal tension at load ratio (characterized by $R = K_{min}/K_{max}$) of 0.05 and 0.75 where K_{min} and K_{max} are the minimum and maximum stress intensities during each cycle. The stress intensity K calibration for the C(T) specimen is expressed as follows [45]:

$$K = \frac{P}{B\sqrt{W}} \frac{(2 + \alpha)}{(1 - \alpha)^{3/2}} (0.886 + 4.64\alpha - 13.32\alpha^2 + 14.72\alpha^3 - 5.6\alpha^4)$$

where P = applied load

B = specimen thickness

W = specimen width, and

α = a/W, the crack length-to-width ratio

expression valid for $a/W \geq 0.2$ [45].

Testing in oils was achieved through immersion of the specimens in the oil contained in a stainless steel chamber which was clamped onto

the bottom grip of MTS load frame. The oil environments were continuously dehumidified *in situ* by bubbling ultrapure dry helium gas through the oil bath, while the whole load frame was sealed using a plastic cover to minimize the contact of oils with the atmosphere of moisture, as shown in Figure 5. Crack growth was continuously monitored using DC electrical potential technique [46,47] capable of detecting increments in crack length of the order of 0.01 mm. Near-threshold growth rates were measured using a load-shedding (decreasing stress intensity) technique in which a procedure of successive load (or ΔK) reduction (initially in decrements of 10% and near ΔK_o, in decrements of 5%) followed by crack growth was performed. In order to minimize premature crack arrest and crack growth retardation effects due to residual compressive stresses generated in front of the crack tip, the crack length increments over which measurements of growth rate are taken were always kept at least four times larger than the plastic zone size generated at the previous load level. The threshold stress intensity, ΔK_o, was defined as the highest alternating stress intensity at which no crack growth could be detected within 10^7 cycles, i.e., in terms of a maximum crack growth rate of 10^{-8} mm/cycle [1].

In order to compare the crack growth behavior in oil and dry helium gaseous environments, constant-load interrupted tests were also performed where the environment was abruptly changed during crack growth at a constant ΔK of 12.3 MPa$\sqrt{m}$, at both low and high load ratios. During each change of oil environment, the residual oil attached on the specimen, especially in the notch root area, was cleaned using organic solvents and compressed air blast.

2.4 ANALYSIS OF FRACTURE SURFACES

2.4.1 Fractography/Scanning Electron Microscopy (SEM)

Fatigue fracture surfaces were examined using AMR-1000 and ISI DS-130 scanning electron microscopes operated at 20 and 25 kV, respectively. The variation in fracture modes at different stress intensity ranges at threshold and higher values ($\sim$ 15 MPa$\sqrt{m}$) in oil environments was examined and compared at approximately mid-thickness of the test pieces.

2.4.2 Auger Electron Spectroscopy (AES)

The determination of oxide thickness on fatigue fracture surfaces in oil environments at R = 0.05 was performed using a PHI Model 590 Auger electron spectroscope. The Fe-O depth composition profiles were obtained as a function of Auger sputtering time, from which the excess oxide thickness (identified as Fe_2O_3) was estimated as a function of crack length using the analytic technique adopted by Suresh et al. [32] on the same steel. Using a beam voltage of 5 kV, ion and electron beam sizes of about 100 and 2 μm, respectively, O and Fe profiles were obtained at a sputtering rate of approximately 150Å/minute. Since the Pilling-Bedworth ratio for iron oxides is approximately 2 [34], the oxide thickness measured on fracture surface represents the excess thickness within the crack assuming only thickness-direction growth. The detailed description of the Auger analysis technique was given in Reference [43].

3. RESULTS

3.1 FATIGUE CRACK PROPAGATION

3.1.1 General Observations

The variation of fatigue crack propagation rates (da/dN) with stress intensity range ($\Delta K = K_{max} - K_{min}$) for SA542-3 steel tested in various oil environments is shown in Figures 6 and 7. Results are compared with the previously obtained data [32] for this steel tested in room temperature moist air (30% relative humidity) and dehumidified gaseous hydrogen and helium environments (both 138 kPa pressure).

It is apparent that at growth rates above 10^{-6} mm/cycle (Fig. 6), the fatigue crack growth rates in oil environments at R = 0.05 are lower than those in moist air and dry hydrogen by up to an order of magnitude and are comparable to those in dry helium gas. Conversely, at near-threshold levels ($\leq 10^{-6}$ mm/cycle), crack growth rates in oils are substantially higher (and threshold ΔK_o values lower) than those in moist air by one to two orders of magnitude with threshold ΔK_o values $\sim$ 30% lower in oil environments and are again comparable to dry gaseous environments.

At R = 0.75 (Fig. 7), crack growth rates above 10^{-7} mm/cycle in silicone oils are lower than in air and dry hydrogen by a factor of about 2.5. However, the crack growth rates in 25 cS paraffin oil in the same growth rate region are interestingly higher than those in silicone oils and are comparable to those in corrosive environments (moist air and dry hydrogen). This is opposite to the observations at R = 0.05 (Fig. 5) where the crack growth rates in paraffin oils can be up to an order of magnitude lower than in silicone oils. In near-threshold

region where the effect of oil is absent, the crack growth rates and the threshold ΔK_o values for both high and low viscosity oil environments as well as moist air and dry hydrogen atmospheres are virtually identical ($\sim$ 3 MPa$\sqrt{m}$) (Fig. 7).

3.1.2 Effects of Oil Viscosity and Chemistry

Figures 8 and 9 show the variation of the crack growth rates (da/dN) with the stress intensity range (ΔK) at R = 0.05 in silicone and paraffin oils, respectively. Crack growth rates above 10^{-6} mm/cycle in both silicone and paraffin oil show a trend to increase with increasing oil viscosity up to a viscosity of 12,500 cS.

The variation in threshold ΔK_o values with increasing kinematic viscosity of the oils is shown in Figure 9. It is apparent that the effect of viscosity on the value of the fatigue threshold ΔK_o is negligible at R = 0.75, whereas at R = 0.05 there is a small but finite trend of decreasing ΔK_o with increasing viscosity in both oils. Furthermore, it is found that the crack growth rates in mid-growth-rate region (i.e., $\sim 10^{-6}$ to 10^{-3} mm/cycle) at R = 0.05 (Fig. 6) in paraffin oils are lower than those in silicone oils even though the viscosities are higher.

The results of constant-stress intensity ($\Delta K \sim$ 12.3 MPa$\sqrt{m}$) interrupted tests in dry helium (138 kPa) and silicone oils on one specimen at R = 0.05 and 0.75 (Fig. 10) show that the crack growth rates at constant stress intensity range (ΔK = 12.3 MPa$\sqrt{m}$ and R = 0.05) (Fig. 10a) is closely related to the change of environment and increase with increasing oil viscosity, with the slowest crack growth in dry helium. The trend, however, is less significant at R = 0.75 (Fig. 10b). It is

evident that the previous observations of the effects of environment and oil viscosity on crack growth behavior (Figs. 6 and 7) are reproducible in a constant-load test on one specimen.

3.1.3 Effect of Load Ratio

The effect of load ratio R (= K_{min}/K_{max}) on crack growth behavior in oil environments is shown in Figure 11. It is clear that crack growth rates in oil environments are increased as load ratio is raised from 0.05 to 0.75 and that such effects are more significant at near-threshold levels. Moreover, it is found that the load ratio effects on the crack growth in silicone oils decrease with increasing oil viscosity (Figs. 11a, b, c), but are much more significant in 25 cS paraffin oil especially at higher growth rates (> 10^{-6} mm/cycle) (Fig. 11d).

3.2 ANALYSIS OF FRACTURE SURFACES

3.2.1 Auger Electron Spectroscopy

Fracture surfaces obtained after fatigue tests in moist environments often show bands of corrosion products in near-threshold region [32]. It was found [32] that the oxide (Fe_2O_3) layer was thickest on specimen tested at low load ratios and was relatively insignificant at high load ratios. The macroscopic appearances of the fatigue fracture surfaces obtained in oil environments and the actual measurements of oxide thickness on the specimens tested in oils and moist air (R = 0.05) [1] as a function of the crack length measured from notch and hence a function of crack growth rate, estimated using Auger electron spectroscopy, are shown in Figures 12 and 13.

The threshold oxide bands on specimens tested at R = 0.05 in oil environments (Fig. 12) are much less visible than the rust-like bands obtained in moist air [32]. The Auger electron spectroscopic analysis (Fig. 13) reveals that the estimated iron oxide thickness near ΔK_o for crack growth in oil environments is uniformly low (∿ 30 Å or 3 nm) compared to much thicker scales observed in moist air (∿ 2000 Å or 200 nm) at near-threshold growth rates (R = 0.05). The threshold data for SA542-3 steel tested in oil environments are listed in Table V.

3.2.2 Fractography

Scanning electron micrographs of representative areas on the fatigue fracture surfaces of SA542-3 steel tested in oil environments at R = 0.05 and 0.75 are shown in Figure 14. At near-threshold stress intensities, fracture morphology at both load ratios shows a typical fine-scale transgranular mode with isolated intergranular facets (Fig. 14a), similar to those previously observed morphology in moist and dry environments [32].

At R = 0.05 and $\Delta K \sim 15$ MPa$\sqrt{m}$, it is found that the typical fracture modes for tests in silicone and paraffin oils are obviously different, with ∿ 30 - 40 percent intergrnaular facets in silicone oils (Fig. 14b) and ∿ 100 percent transgranular mode in paraffin oils (Fig. 14c). However, at R = 0.75 and $\Delta K \sim 15$ MPa$\sqrt{m}$, a large proportion of intergranular fracture mode is observed in both oils. The proportion of intergranular facets in paraffin oil is increased to about 80 percent (Fig. 14e) but with no appreciable change in silicone oils as load ratio increases (Fig. 14d).

4. DISCUSSION

4.1 VISCOUS FLUID-INDUCED PROTECTIVE EFFECTS

Current studies on fatigue crack propagation in SA542-3 steel have shown that dehumidified oil environments can influence behavior in two distinct crack growth rate regions at low load ratios (Figs. 6 and 8), compared with the earlier data curves obtained in various moist and dry environments by Suresh et al. [32]. At near-threshold levels where crack growth rates are typically below 10^{-6} mm/cycle, crack growth rates in dehumidified oil environments were higher (and threshold ΔK_o values lower) than those in moist environments (i.e., room air, distilled water and wet hydrogen), yet were comparable to growth rates in dry environments (i.e., dry hydrogen and dry helium). Conversely, at higher stress intensities or at crack growth above 10^{-6} mm/cycle, crack growth rates in oil environments were substantially lower than those in moist environments and dry hydrogen, but again were comparable to those in dry helium.

Explanations for similar observations in two 2¼Cr-1Mo steels (i.e., ASTM A387 class 2 grade 22 and currently-used SA542-3) tested in moist and dry environments have been made by Ritchie et al. [28] and Suresh et al. [32] in terms of a competition between two concurrent processes, namely crack closure due to corrosion debris formed on the fracture surfaces [29,48-50,62], i.e., oxide-induced crack closure [28,31-32] (which decreases growth rates and increases the threshold ΔK_o) and hydrogen embrittlement arising from the production of hydrogen vis-a-vis the oxidation process (which increases growth rates and decreases the threshold ΔK_o). Since in lower strength steels tested at high

frequencies, e.g., 50 Hz, the conventional corrosion fatigue processes (i.e., hydrogen embrittlement and/or active path corrosion) are less effective, it has been observed [28,32] that closure phenomena, particularly oxide-induced crack closure, appear to dominate overall near-threshold fatigue crack growth behavior. Accordingly, crack growth rates at near-threshold levels were found to be significantly faster at low load ratios in dry environments than in wet environments. However, in mid-growth region ($da/dN > 10^{-6}$ mm/cycle) where conventional corrosion fatigue mechanisms are effective [51], crack growth rates were much lower in inert dry environments, such as dry helium gas, than those in corrosive environments, such as wet media and dry hydrogen.

In addition to the aforementioned observations, Holshouser and Utech [52] observed that the fatigue crack propagation rates in some alloys, such as high-strength 4340 steel, 17-7 PH stainless steel, 6061-T6 Al alloy and a copper-beryllium alloy, were reduced by coating the specimens with dodecyl alcohol which could form an organic oleophobic film on metal surfaces and then concluded that the reduction of crack growth rates was mainly attributed to the exclusion of oxygen and moisture from these materials by those oleophobic films. Ryder et al. [8] stated that inert liquid environments, such as dodecanol decane, silicone oil, and grease, decreased the Stage II fatigue crack growth in two Al-Zn-Mg alloys by excluding air from crack regions and enhanced Stage I crack growth probably by hydraulic removal of fretting products from the crack. Moreover, a considerable amount of studies on the fatigue behavior of various kinds of metallic materials [13,53-60] have confirmed that moisture or water vapor existing in moist atmospheres

is the primary supplier of harmful species, especially hydrogen, which enhances fatigue crack propagation mainly through hydrogen embrittlement mechanism as a result of oxidation reaction taking place in the crack tip region. The results of current studies on SA542-3 steel tested in dehumidified oil environments at both low and high load ratios are consistent with these observations and indicate that the principal function of the oil environment is to serve as a physical barrier to the embrittling species (i.e., moisture) to the crack tip region, i.e., to behave like dry or inert environment.

Quantitative analysis of the fracture surfaces using Auger electron spectroscopy which has recently been adopted to measure the excess oxide thickness on the near-threshold fatigue fracture surfaces [32,39,61-63] showed that the thickness of crack surface oxide scales near ΔK_o for crack growth in oil environments at R = 0.05 was uniformly low (∿30Å or 3 nm) compared to much thicker scales observed in room air (∿2000Å or 200 nm) at the same load ratio (Fig. 13) and became a strong supporting evidence for the protective effects due to oil environments. According to the oxide-induced crack closure model [32], the oxide layers can cause premature contact of crack surfaces during the unloading part of a stress cycle at near-threshold levels where cyclic crack tip opening displacements are small and result in a reduced ΔK value actually experienced at the crack tip, namely $\Delta K_{eff} = K_{max} - K_{cl}$, where K_{cl} is the stress intensity at which crack closes.

Suresh et al. [31,34] treated the crack surface oxide as an ideal rigid body (Fig. 15) and calculated the closure stress intensity K_{cl} at the crack tip due to oxide wedging using the following expression for

closure stress intensity under plane strain conditions

$$K_{cl} = \frac{D\,E}{4\sqrt{\pi \ell}\,(1 - \nu^2)} \qquad (1)$$

where D is the maximum excess oxide thickness located at a distance 2ℓ from the crack tip, E the Young's modulus, and ν the Poisson's ratio. Taking $\ell \sim 2$ μm, they found the calculated difference in closure stress intensity due to different oxide thicknesses between tests (R = 0.05) in moist air and dry hydrogen at threshold levels were approximately equal to the difference in observed threshold ΔK_o values (~ 2 MPa$\sqrt{m}$). Now, based on the same assumptions, the estimated stress intensity increment for tests in oil environments with a maximum oxide thickness of d $\sim$ 30Å (Fig. 13) is about 0.1 MPa$\sqrt{m}$, compared to 4.5 and 2.3 MPa$\sqrt{m}$ for moist air and dry hydrogen, respectively. It is apparent that the crack closure due to the existence of oxide debris is substantially minimized in oil environments. Thus, the role of dehumidified oil environments in influencing *near-threshold* fatigue crack growth can be explained. The protective effects and the limited oxide formation on crack surfaces due to oil environments lead to lower crack growth rates (compared to corrosive environments, such as wet environments and dry hydrogen) above typically 10^{-6} mm/cycle where conventional corrosion fatigue processes contribute to crack growth, and to faster crack growth rates at near-threshold levels.

At R = 0.75 and above 10^{-6} mm/cycle (Fig. 7), the lower crack growth rates in silicone oils compared to air and dry hydrogen can also be attributed to the protective effects provided by the oil environments. Since the enhanced oxide formation by fretting oxidation mechanisms [29]

and closure mechanisms in general are relatively insignificant at high load ratios, near-threshold crack growth behavior in oils, air and hydrogen tend to be similar (Fig. 7), with approximately the same threshold ΔK_0 value ($\sim$ 3 MPa$\sqrt{m}$). It is clear that the concept of oxide-induced crack closure appears to be able to successfully demonstrate the general near-threshold fatigue crack growth behavior of SA542-3 steel not only in moist, dry and inert environments, but in oil environments as well. Therefore, based on the above discussion, the observed enhancement of Stage I fatigue crack growth in non-corrosive fluids would be likely to result from the shielding effects provided by the fluids rather than from the "hydraulic removal" of the fretting debris [8]. Furthermore, it will be shown later that the entering of fluids into Stage I cracks is extremely limited such that any fluid flow responsible for the removal of fretting products from the cracks is unlikely to occur.

4.2 VISCOUS FLUID-INDUCED CRACK CLOSURE

4.2.1 Effect of a Hydrodynamic Wedge

Suppose a certain amount of viscous fluid is trapped in a fatigue crack, it is not hard to imagine that the fluid will act as a cushion or a wedge as the crack closes at a sufficiently high speed and will probably affect the fatigue crack growth behavior. It has been mentioned that most of the studies [5,6,15-24] showed that the fatigue lives of (or fatigue crack propagation rates in) metallic materials tested in oil are increased with increasing oil viscosity. With regard to the viscosity effects, following Way's [25] fluid penetration and hydraulic pressure mechanisms, Galvin and Naylor [23] subsequently stated that the pressure

generated by the fluid confined in a crack was considered to be relevant to the physical properties of fluids, such as viscosity, viscosity-pressure coefficient, compressibility, etc., and that the higher the pressure the faster the crack would grow. However, no quantitative analyses of the pressure mechanism were made by these investigators and their explanations were also questionable from fracture mechanics viewpoints. Since it is well known that the primary effect of crack closure on fatigue crack propagation is to reduce the driving force or stress intensity range responsible for crack extension from ΔK (= $K_{max} - K_{min}$) to ΔK_{eff} (= $K_{max} - K_{cl}$) due to premature contact of crack faces at positive external applied load and hence lower the fatigue crack propagation rates. Consequently, without considering chemical effects, any mechanical factors, such as the oxide and hydrodynamic wedge actions, which can cause fatigue crack closure or, say, reduction of stress intensity range ΔK, are expected to reduce rather than to increase the fatigue crack growth rates.

According to the studies by Endo and his co-workers [5,6], the fatigue crack propagation in both ferrous [6] and non-ferrous alloys [5] in oil environments were affected by the wedge action of oil trapped in the crack during the unloading part of stress cycles. Their results showed that the rates of fatigue crack growth in a medium carbon steel tested in silicone and paraffin oils also *decreased* with increasing viscosity. However, the current studies on SA542-3 steel tested at R = 0.05 in similar oil environments at 50 Hz (Figs. 6 and 8) indicated crack growth rates to be marginally *higher* in the higher viscosity oils at both near-threshold and higher growth rates.

Despite the apparent discrepancies, Endo et al. [5] quantified the oil wedging action using the following expression for the oil pressure distribution within a closing fatigue crack, based on the assumption that oil could fully fill the crack, as shown in Figure 16:

$$p(x) = \frac{6\eta\rho a^3}{h^3}\frac{d\theta}{dt}\log(1 - \frac{x}{a}) \qquad (2)$$

where p(x) is the hydrodynamic oil pressure depending on the position between the crack tip and mouth while crack closes with an angular velocity $d\theta/dt$ at the crack mouth opening displacement h, η the kinematic viscosity, ρ the density of oil and a the crack length. The problem with this full penetration model is that lower ΔK levels and high frequencies, the crack opening widths are so small (of the order of microns) that it is improbable that viscous fluids will fully penetrate into the crack naturally without external force. The extent of fluid penetration into a crack is thus of importance in determining the extent of closure. However, this aspect has been ignored in almost all of the previous modelling studies reported. Furthermore, previous models have not been analyzed for the hydrodynamic wedge effect on the fatigue crack growth in terms of fracture mechanics. In the present work, a new model for characterizing the crack closure during fatigue crack growth in viscous fluid environments is proposed based on a fracture mechanics analysis of hydrodynamic wedging effects from partial penetration of oil into the crack.

Since hydrodynamic pressure is generated as crack closes, linear superposition methods indicate that the linear elastic stress intensity actually experienced at the crack tip at applied K_{min} will be raised to

K_{cl}^{w}, where K_{cl}^{w} is the closure stress intensity due to hydrodynamic wedge effect. Hence, nominal ΔK (= $K_{max} - K_{min}$) reduced to effective value ΔK_{eff} (= $K_{max} - K_{cl}^{w}$) by an amount K_p resulting from such pressure, where K_p is the stress intensity increment as a result of the hydrodynamic wedge action. This concept is demonstrated in Figure 17. Based on Endo et al.'s full penetration model (Eq. 2), the magnitude of the hydrodynamic pressure and hence K_p will be proportional to the oil viscosity at constant crack length, stress frequency and amplitude, showing qualitative consistence with their experimental results [5,6]. Now we assume that the depth of fluid penetration is reasonably governed by the capillary actions and will determine the effectiveness of the hydrodynamic wedge on influencing crack growth behavior. In this case, assume the ratio of the penetration distance (d) to the crack width (B) is small (Fig. 18) so that the fluid within the crack will not flow in the thickness direction, i.e., the z-direction, when the fluid is squeezed as crack closes. Then, the real fluid pressure distribution based on ref. 64 is approximately given by

$$p(x) = -\frac{6\eta\rho v x}{H^3}(x - d) \tag{3}$$

where H is the average crack opening width at closing velocity v. The profile for the pressure distributions in a crack, based upon Eqs. 2 and 3, are shown in Figures 16 and 18.

Considering an idealized fatigue crack of uniform rectangular cross-section having length a, width B and average crack opening H, and assuming fluid only enters the crack from the notch during the opening half cycles (Fig. 19), the penetration distance (d) can be estimated

using Newman's [42] capillary flow equations as

$$d \sim \left(\frac{H\gamma_L \cos\beta}{6\eta\rho f}\right)^{\frac{1}{2}} \tag{4}$$

where γ_L is the surface tension of fluid, β the wetting angle between fluid and crack walls, and f the cyclic frequency. Assume the overall shape of the crack to be trapezoidal with the displacement h at the crack mouth and δ at the crack tip, using Turnbull's [65] calculation for the average crack opening width of compact tension specimen, the average crack opening width for an edge crack will be

$$H = \tfrac{1}{2}(h + \delta) \tag{5}$$

If treating cyclically-loaded cracks as static ones with crack opening width independent of time, the simplified average crack opening width can be approximated as follows:

$$\bar{H} = \tfrac{1}{2}(H_{max} + H_{min}) \tag{6}$$

$$= \tfrac{1}{4}(h_{max} + \delta_{max} + h_{min} + \delta_{min}) \tag{7}$$

Assume the rotational axis of a fatigue-cracked specimen is at a position rb to the right of the crack tip (Fig. 19), where r is the rotational factor determining the location of the apparent rotational axis in the specimen ligament b (= W - a) along crack line, usually varying from $\sim$ 0.195 in elastic situation to $\sim$ 0.47 in plastic situation [66], then the relationship between h and δ can be expressed as

$$h = \frac{a + rb}{rb}\,\delta \tag{8}$$

Taking δ, the crack tip opening displacement, = 0.49 (K^2/YE) [1], where K is the applied stress intensity factor, Y the yield strength, and E the Young's modulus, Eq. 7 becomes

$$\bar{H} = \frac{1}{8}\left(2 + \frac{a}{rb}\right) \frac{\Delta K^2}{YE} \frac{1 + R^2}{(1 - R)^2} \tag{9}$$

where R is load ratio $(= K_{min}/K_{max})$. Combining Eqs. 4 and 9, the fluid penetration distance into an edge fatigue crack is approximately

$$d \sim \left[\frac{\gamma_L \cos\beta}{48\eta\rho f} \left(2 + \frac{a}{rb}\right) \frac{\Delta K^2}{YE} \frac{1 + R^2}{(1 - R)^2}\right]^{\frac{1}{2}} \tag{10}$$

It is now apparent that the constant frequency, crack length, stress amplitude and load ratio, the extent of the penetration of oils with similar surface properties (e.g., surface tension, contact angle, etc.) and densities is mainly determined by the viscosity of oils.

4.2.2 Estimation of the Closure Stress Intensity (K^W_{cl}) Due to Hydrodynamic Wedge Actions

Owing to the existence of hydrodynamic wedging effects, the crack faces are expected to stop closing before reaching the minimum load during the unloading part of a cycle, showing an equivalent crack closure mechanism, namely viscous fluid-induced crack closure.

Firstly, for the case of partial penetration (Fig. 18), assuming the crack walls approaching at a constant velocity when they close, the equivalent resultant force (per unit thickness) in MN/m for the parabolic pressure distribution (Eq. 3) at minimum applied load (or K_{min}) can be expressed as

$$F_p^e = 3.2 \times 10^{-8}\, \eta\rho f d^3 \frac{a + rb}{(a + 2rb)^3} \left(\frac{YErb}{\Delta K^2}\right)^2 \left(\frac{1 - R}{R}\right)^6 \tag{11}$$

where the superscript e and the subscript p stand for 'edge crack' and 'partial penetration', respectively. The detailed derivation of Eq. 11 is given in Appendix A. Since the centroid of the parabolic pressure distribution is at x = d/2 (Fig. 18a), the calculation by using Sih's [67] solution to an edge crack subjected to concentrated forces yields an approximate stress intensity increment experienced at the crack tip as follows:

$$K_p^e = \frac{2Q}{\sqrt{\pi a}} F_p^e \tag{12}$$

where Q is the geometric factor given in terms of the ratio of the penetration distance to the crack length ε (= d/a),

$$Q = \frac{C(\varepsilon)}{\sqrt{1 - (\varepsilon/2)^2}}$$

where

$$C(\varepsilon) = 1.2945 - 0.1473\varepsilon - 0.0978\varepsilon^2 + 0.0489\varepsilon^3 + 0.048\varepsilon^4 - 0.024\varepsilon^5 - 0.0155\varepsilon^6 + 0.0078\varepsilon^7 + 0.002\varepsilon^8 - 0.001\varepsilon^9$$

However, for a compact tension testpiece (Fig. 3) with a growing fatigue crack, the effective hydrodynamic oil pressure contributing to the fluid-induced crack closure effect is expected to be generated only in the 'effective' penetration distance d_{eff} measured from the notch root as indicated in Figure 18b. In this situation, Eqs. 10 to 12 can, therefore, be modified into the following by replacing a with $a - a_o$:

$$d_{eff} \sim \left(\frac{\gamma_L \cos\beta\, \Delta K^2}{48\eta\rho f Y E} \left(2 + \frac{a - a_o}{rb}\right) \frac{1 + R^2}{(1 - R)^2}\right)^{1/2} \tag{13}$$

$$F_p^c = 3.2 \times 10^{-8}\ \eta\rho f d_{eff}^3 \frac{a - a_o + rb}{(a - a_o + 2rb)^3} \left(\frac{YErb}{\Delta K^2}\right)^2 \left(\frac{1 - R}{R}\right)^6 \tag{14}$$

$$K_p^c = \frac{2Q'}{\sqrt{\pi a}} F_p^c \tag{15}$$

where the superscript c stands for 'CT specimen', a_o the initial crack length or the notch depth of the CT specimen, Q' the geometric factor determined by

$$Q' = \frac{G(\phi)}{\sqrt{1 - \phi^2}}$$

where $\phi = c/a$, and c $(= a_o + \frac{d_{eff}}{2})$ is the distance between the centroid of the effective distributed hydrodynamic pressure and the loading line of the CT specimens, and

$$G(\phi) = 1.2945 - 0.2945\phi - 0.3912\phi^2 + 0.3912\phi^3 + 0.7685\phi^4 - 0.7685\phi^5 - 0.9942\phi^6 + 0.9942\phi^7 + 0.5094\phi^8 - 0.5094\phi^9$$

Secondly, provided that the capillary action is not considered, the calculations of the stress intensity increment using Endo's oil pressure model (Fig. 16 and Eq. 2) and performing the same analyses as above generate the following results:

1) For an edge crack, the stress intensity increment at K_{min} due to oil wedge is

$$K_f^e = 1.8595\ P_f^e \sqrt{a} \tag{16}$$

where

$$P_f^e = 1.1 \times 10^{-8}\ \eta\rho f \left(\frac{a}{a + rb}\right)^3 \left(\frac{YErb}{\Delta K^2}\right)^2 \left(\frac{1 - R}{R}\right)^6 \tag{17}$$

2) For CT specimens:

$$K_f^c = \frac{2Q''}{\sqrt{\pi a}} P_f^c (a - a_o) \tag{18}$$

where

$$P_f^c = 1.1 \times 10^{-8} \eta \rho f \left(\frac{a - a_o}{a - a_o + rb}\right)^3 \left(\frac{YErb}{\Delta K^2}\right)^2 \left(\frac{1 - R}{R}\right)^6 \tag{19}$$

$$Q'' = \frac{G(\tau)}{\sqrt{1 - \tau^2}}$$

where

$$\tau = \tfrac{1}{2}\left(3 + \frac{a_o}{a}\right)$$

where the subscript f stands for 'full penetration.' The detailed derivation of Eq. 17 is given in Appendix B.

According to the above analyses, under the same mechanical conditions, it is not hard to find that for cases of partial penetration (Eqs. 12 and 15) the fluid-induced stress intensity increments K_p^e and K_p^c are inversely proportional to $\eta^{-\frac{1}{2}}$, resulting in increasing ΔK_{eff} (and hence increasing crack growth rates and decreasing fatigue lives) with increasing fluid viscosity. However, for cases of full penetration (Eqs. 16 and 18), the stress intensity increments K_f^e and K_f^c are proportional to η, resulting in decreasing ΔK_{eff} (and hence decreasing crack growth rates and increasing fatigue lives) with increasing viscosity. It is therefore clear that the presence and absence of capillary action can lead to two totally opposite dependences of the hydrodynamic wedge action on the fluid viscosity. Hence, the above-stated theoretical rationalization through a combination of fracture mechanics, capillary flow and hydrodynamic concepts may be able to

explain the reason why there have been diversely observed variations of fatigue behavior with the viscosity of environmental fluids so far.

To quantify the significance of viscous fluid-induced crack closure, we use the above models and take currently used SA542-3 steel CT specimens with rotational factor $r \sim 0.4$ [68] and crack length $a \sim 25$ mm for tests in silicone and paraffin oils ($f = 50$ Hz, $\Delta K = 10$ MPa$\sqrt{m}$. Assuming the same estimated wetting angles ($\sim 10°$) at $R = 0.05$ and 0.75, the calculations of the magnitude of the closure stress intensity K^{W}_{cl} using the full penetration model (Eq. 18) indicate that the closure stress intensity K^{W}_{cl} values are too large to be acceptable. However, the calculations using the currently proposed partial penetration model (Eq. 15) predict, *without any recourse to the use of adjustable parameters*, reasonable closure stress intensity K^{W}_{cl} values (Table VI) and show that at $R = 0.05$ and higher growth rates the oil penetration into the crack is highly restricted for the higher viscosity (e.g., 1000-60,000 cS) oils due to the small crack opening widths, partial oil penetration into the crack can result in additional crack closure for oils of lower viscosity. Accordingly, crack growth rates between $\sim 10^{-6}$ and 10^{-5} mm/cycle in the paraffin oils and 5 cS silicone oil were actually slower than in dry helium gas (Fig. 6) indicating that both environmental shielding effects and viscous fluid-induced crack closure mechanisms were active. At $R = 0.75$, the estimated penetration depths for both low and high viscosity oils are ~ 5 times larger than those at $R = 0.05$ due to a 25-fold increase of average crack opening displacements. However, this much larger crack opening yields minimal pressure such that oil pressure induced crack closure is infinitesimal (Table VI)

and corresponding little effect of oil viscosity is observed (Fig. 7). The comparison of quantitative extent of viscous-fluid-induced crack closure based on current partial penetration model (Table VI) and Endo and co-workers' full penetration model is shown in Table VII.

Finally, a few points associated with the above analyses are worthy of note. Firstly, it is well known that the viscosity of fluids usually increase with increased ambient pressure. The viscosity-pressure coefficient* of fluids will determine the extent of the viscosity change with the variation of the ambient pressure. In other words, with similar penetration depths and under the same mechanical conditions, fluid with larger viscosity-pressure coefficient tends to generate a *larger* hydrodynamic pressure inside the crack and hence a *smaller* effective driving force (ΔK_{eff}) for fatigue crack growth. Compared with silicone oils, paraffin oils have larger viscosity-pressure coefficients [6]. This may explain why the crack growth rates are lower in paraffin oils (Fig. 6) even though the calculated fluid-induced closure stress intensities (K^{w}_{cl}) are comparable to those for 5 cS silicone oil (Table VI). Secondly, there is always a possibility that active constituents in the oil might give rise to some environmentally-assisted contribution to crack growth. For example, Swets and Frank [69] showed that the hydrogen originally included in the hydrocarbon constituents of the lubricants may be absorbed by steel parts operated in the lubricant and

---

*The viscosity-pressure relationship can be expressed as

$$\ln \frac{\eta}{\eta_o} = \psi P$$

where η_o is the original viscosity, ψ the viscosity-pressure coefficient.

cause detrimental effects, such as hydrogen embrittlement. The abnormally higher crack growth rates above 10^{-6} mm/cycle observed in 25 cS paraffin oil compared to those in silicone oils at R = 0.75 (Fig. 7) may be a result of this effect, since a larger percentage ($\sim$ 80%) of intergranular facets which were not seen in silicone oils (Fig. 14d) was observed on the fracture surfaces obtained in 25 cS paraffin oil (Fig. 14e).

Thus, any factor which can affect the extent of oil penetration and the magnitude of hydrodynamic oil pressure or change the local environment near the crack tip, such as a) the crack opening displacements, b) the viscosity-pressure characteristics, c) the composition, d) the chemical stability of the environmental oils, e) the relative motions between the cracked components and the environmental oils (e.g., the rolling of bearing balls in lubricating oils), f) the growing orientation of the crack relative to that of the ambient gravity field [70] in different types of specimens (e.g., rotating beam, single-edge notch, or CT specimens), g) the external pressure applied to the environmental oils, etc., may lead to different observations of the variation of crack growth behavior with any specific physical properties of interest. But undoubtedly, based on the present studies, for fatigue cracks growing in dehumidified viscous environments, the viscosity and viscosity-related properties of the fluid which dominate the penetration mechanisms and therefore the hydrodynamic wedging effects, play the more important roles in determining the crack growth behavior under various mechanical situations.

4.3 Effect of Load Ratio (or Mean Stress)

In studies of fatigue crack propagation, the load ratio R (= K_{min}/K_{max}) is always considered to be of great importance. Generally speaking, the load ratio effects are minimal in the mid-growth-rate regions (typically 10^{-6} to 10^{-3} mm/cycle) but are significantly relevant at near-threshold levels (< 10^{-6} mm/cycle) with the threshold stress intensity ΔK_o value obviously decreased and crack growth rates increased as R is raised [1].

In the previous studies on SA542-3 steel tested in moist air and dry hydrogen (50 Hz) at room temperature [32], it was observed that growth rates were insensitive to load ratio above 10^{-5} mm/cycle, whereas at near-threshold levels growth rates were largely increased, and threshold ΔK_o values markedly decreased, with increasing load ratio. However, in the present investigation the latter trend was again observed in near-threshold region (Fig. 11) although it became smaller due to the minimization of oxide-induced crack closure at low load ratios. Moreover, the R effects seemed to be dependent on the type and viscosity of the environmental oils in mid-growth-rate region and were more visible for lower viscosity oils.

It is recalled that the stress intensity increments at higher growth rates (> 10^{-6} mm/cycle) due to the partial oil penetration, K_p^e and K_p^c, are proportional to the resultant hydrodynamic forces, F_p^e and F_p^c, respectively (Eqs. 12 and 15). Since the penetration distances and the hydrodynamic forces are proportional to the complex functions of oil viscosity (η) and R as

$$d \text{ or } d_{eff} \propto \left(\frac{1 + R^2}{\eta(1 - R)^2}\right)^{\frac{1}{2}} \qquad \text{(Eqs. 10 and 13)}$$

$$\left.\begin{matrix} p_p^e \\ p_p^c \end{matrix}\right\} \propto \left\{\begin{matrix} \eta d^3\left(\frac{1 - R}{R}\right)^6 \\ \eta d_{eff}^3\left(\frac{1 - R}{R}\right)^6 \end{matrix}\right. \qquad \text{(Eqs. 11 and 14)}$$

such that

$$K_p^e \text{ or } K_p^c \propto \eta^{-\frac{1}{2}}\left(\frac{(1 - R)(1 + R^2)^{\frac{1}{2}}}{R^2}\right)^3 \qquad (20)$$

At constant viscosities, both K_p^e and K_p^c thus decrease as load ratio increases, indicating that the load ratio effects are more marked in lower viscosity oils. The current results (Fig. 11), showing the increasing R effect on higher growth rates with decreasing oil viscosity, are quite consistent with the above rationalization. However, it has to be noted that the marked R effect observed in 25 cS paraffin oils (Fig. 11d) was possibly due to an unexpected decomposition of its constituents. Therefore, the load ratio effects on fatigue crack propagation in dehumidified viscous environments are apparently complicated by several mechanisms, such as the minimization of oxide-induced crack closure, the hydrodynamic wedging effects of the viscous fluid within the crack, and the probable local environmental change near the crack tip due to unanticipated chemical degradation of the viscous fluids. The complex characteristics of fatigue crack propagation in viscous environments at intermediate and near-threshold growth rates are summarized in Table VIII.

5. CONCLUSIONS

Based on a study of the effect of dehumidified viscous environments on the ambient temperature fatigue crack propagation behavior in bainitic 2¼Cr-1Mo pressure vessel steel (ASTM A542 Class 3), the following conclusions can be made:

1) The role of the dehumidified viscous environments in fatigue crack propagation in lower strength steels was apparent in two distinct growth rate regions, namely at the mid-range of growth rates (typically above $\sim 10^{-6}$ mm/cycle) and at near-threshold levels ($\leq 10^{-6}$ mm/cycle).
2) In mid-growth-rate region ($\sim 10^{-6}$ to 10^{-3} mm/cycle), growth rates in dry oil environments were *lower* than those in moist air and dry hydrogen by up to an order of magnitude at both low and high load ratios and are comparable to those in dry helium gaseous environment.
3) In near-threshold region, growth rates at R = 0.05 in dry oil environments were *higher* than those in moist air by up to two orders of magnitude and comparable to those in dry hydrogen and helium gases, with the threshold ΔK_o values approximately 30 percent lower in oil environments. At R = 0.75, growth rates and ΔK_o values were identical in oils, air and dry hydrogen.
4) At R = 0.05, crack growth rates above 10^{-6} mm/cycle in both silicone and paraffin oils increased with increasing oil viscosity and became unchanged when viscosity reached 12,500 cS

(in this study). The effect of oil viscosity was absent at near-threshold levels, although there was a small but finite decrease in ΔK_o values with increasing viscosity. At R = 0.75, no effect of oil viscosity was observed in both mid-growth-rate and near-threshold regions.

5) The crack growth rates in oil environments were increased as load ratio increased from 0.05 to 0.75 in both near-threshold and mid-growth-rate regions. It was found that the load ratio effect was more significant for lower viscosity oils.

6) The crack growth rates above 10^{-6} mm/cycle at low load ratios in paraffin oils were lower than those in silicone oils of comparatively lower viscosities. It probably resulted from that the paraffin oils have higher surface tension and viscosity-pressure indices which tended to enhance the hydrodynamic wedging effects.

7) The complex fatigue crack growth characteristics in dry viscous environments could be rationalized in terms of three mutually competitive mechanisms: suppression of moisture-induced hydrogen embrittlement and/or metal dissolution, minimization of oxide-induced crack closure and hydrodynamic wedging effects of the viscous fluid within the crack.

8) A new quantitative model termed *viscous fluid-induced crack closure* characterizing the hydrodynamic wedge action of viscous fluid within a fatigue crack was developed based on partial penetration phenomena through the combination of fracture mechanics, capillary flow and hydrodynamic analysis. The

effects of viscosity and load ratio on the fatigue crack growth in viscous environments were predicted using this model.

REFERENCES

1. R. O. Ritchie, "Near-Threshold Fatigue-Crack Propagation in Steels," Int. Met. Rev., 20, 1979, 205-230.
2. P. C. Paris and F. Erdogan, "A Critical Analysis of Crack Laws," J. Basic Eng., Trans. ASME, Series D, 85, 1963, 528-534.
3. R. O. Ritchie and J. F. Knott, "Mechanisms of Fatigue Crack Growth in Low Alloy Steel," Acta Met., 21, 1973, 639-648.
4. N. E. Frost, "The Effect of Environment on the Propagation of Fatigue Cracks in Mild Steel," Appl. Mat. Res., 3, 1964, 131-138.
5. K. Endo, T. Okada and T. Hariya, "Fatigue Crack Propagation in Bearing Metals Lining on Steel Plates in Lubricating Oil," Bull. JSME, 15, 1972, 439-445.
6. K. Endo, T. Okada, K. Komai and M. Kiyota, "Fatigue Crack Propagation of Steel in Oil," Bull. JSME, 15, 1316-1323.
7. C. J. Polk. W. R. Murphy and C. N. Rowe, "Determining Fatigue Crack Propagation Rates in Lubricating Environments through the Application of a Fracture Mechanics Technique," ASLE Trans., 18, 1975, 290-298.
8. D. A. Ryder, M. Martin and M. Abdullah, "Some Factors Influencing Stage I Fatigue-Crack Growth," Met. Sci., 11, 1977, 340-344.
9. L. Grunberg and D. Scott, "The Acceleration of Pitting Fracture by Water in the Lubricant," J. Inst. Petrol., 44, 1958, 406-410.
10. P. Schatzberg and I. M. Felson, "Effects of Water and Oxygen During Rolling Contact Lubrication," Wear, 12, 1968, 331-342.

11. J. A. Ciruna and H. J. Szieleit, "The Effect of Hydrogen on the Rolling Contact Fatigue Life of AISI 52100 and 440C Steel Balls," Wear, 24, 1973, 107-118.

12. C. J. Polk and C. N. Rowe, "Crack Growth Rate: Its Measurement and a Controlling Factor in Rolling Contact Fatigue," ASLE Trans., 19, 1976, 23-32.

13. R. E. Cantley, "The Effect of Water in Lubricating Oil on Bearing Fatigue Life," ASLE Trans., 20, 1977, 244-248.

14. O. Vosikovsky, "Fatigue Crack Growth in an X65 Line-Pipe Steel in Sour Crude Oil," Corrosion, 32, 1976, 472-475.

15. O. Vosikovsky and A. Rivard, "The Effect of Hydrogen Sulfide in Crude Oil on Fatigue Crack Growth in a Pipe Line Steel," Corrosion, 38, 1982, 19-22.

16. M. E. Otterbein, "The Effect of Gas Turbine Oil on Roller Bearing Fatigue Life," ASLE Trans., 1, 1958, 33-39.

17. W. J. Anderson and T. L. Carter, "Effect of Lubricant Viscosity and Type on Ball Fatigue Life," ASLE Trans., 1, 266-272.

18. J. B. Martin and A. Cameron, "Effect of Oil on the Pitting of Rollers," J. Mech. Eng. Sci., 3, 1961, 148-152.

19. F. G. Rounds, "Effects of Base Oil Viscosity and Type on Bearing Ball Fatigue," ASLE Trans., 5, 1962, 172-182.

20. W. E. Littmann, R. L. Widner, J. O. Wolfe and J. D. Stover, "The Role of Lubrication in Propagation of Contact Fatigue Cracks," J. Lubric. Tech., Trans. ASME, Series F, 90, 1968, 89-100.

21. F. G. Rounds, "Lubricant and Ball Steel Effects on Fatigue Life," J. Lubric. Tech., Trans. ASME, Series F, 93, 1971, 236-245.

22. F. G. Rounds, "Base Oil Effects on Fatigue Life for Additive Blends as Measured on a 4-Ball Fatigue Machine," ASLE Trans., 20, 1977, 115-125.

23. G. D. Galvin and H. Naylor, "Effect of Lubricants on the Fatigue of Steel and Other Metals," Proc. Instn. Mech. Engrs., 179, 1964-65, 857-875.

24. I. Koved, "The Effect of Three Mineral Base Oil on Roller Bearing Fatigue Life," ASLE Trans., 9, 1966, 222-228.

25. S. Way, "Pitting Due to Rolling Contact," J. Appl. Mech., Trans. ASME, Series E, 2, 1935, A49-A114.

26. W. Elber, "The Significance of Fatigue Crack Closure," in Damage Tolerance in Aircraft Structures, ASTM STP 486, Amer. Soc. Test. Mat., 1971, 230-242.

27. W. Elber, "Fatigue Crack Closure Under Cyclic Tension," Eng. Fract. Mech., 2, 1970, 37-45.

28. R. O. Ritchie, S. Suresh and C. M. Moss, "Near-Threshold Fatigue Crack Growth in 2¼Cr-1Mo Pressure Vessel Steel in Air and Hydrogen," J. Eng. Mat. Tech., Trans. ASME, Series H, 102, 1980, 293-299.

29. D. Benoit, R. Namdar-Irani and R. Tixier, "Oxidation of Fatigue Fracture Surfaces at Low Crack Growth Rates," Mat. Sci. Eng., 45, 1980, 1-7.

30. A. T. Stewart, "The Influence of Environment and Stress Ratio on Fatigue Crack Growth at Near-Threshold Stress Intensity in Low-Alloy Steels," Eng. Fract. Mech., 13, 1980, 463-478.

31. S. Suresh, D. M. Parks and R. O. Ritchie, "Crack Tip Oxide Formation and Its Influence on Fatigue Thresholds," in Fatigue Thresholds, ed. by J. Bäcklund, A. Blom and C. J. Beevers, EMAS Ltd., Warley, U.K., 1982, Vol. 1, 391-408.

32. S. Suresh, G. F. Zamiski and R. O. Ritchie, "Oxide-Induced Crack Closure: An Explanation for Near-Threshold Corrosion Fatigue Crack Growth Behavior," Metall. Trans. A, 12A, 1981, 1435-1443.

33. S. Suresh and R. O. Ritchie, "Mechanistic Dissimilarities Between Environmentally-Influenced Fatigue Crack Propagation at Near-Threshold and Higher Growth Rates in Lower Strength Steels," Met. Sci., 16, 1982, 529-538.

34. S. Suresh and R. O. Ritchie, "Some Considerations on the Modelling of Oxide-Induced Fatigue Crack Closure Using Solutions for a Rigid Wedge Inside a Linear Elastic Crack," Scripta Met., 17, 1983, 575-580.

35. G. Sewell and H. L. Marcus, "A Model for Fatigue Crack Closure Based on Surface Roughness and Residual Strain," Scripta Met., 11, 1977, 521-524.

36. N. Walker and C. J. Beevers, "A Fatigue Crack Closure Mechanism in Titanium," Fatig. Eng. Mat. Struct., 1, 1979, 135-148.

37. I. C. Mayes and T. J. Baker, "Load Transference Across Crack Faces During Fatigue Crack Growth at Positive Values of R in Low Growth Rate Regime," Met. Sci., 15, 1981, 320-322.

38. K. Minakawa and A. J. McEvily, "On Crack Closure in the Near-Threshold Region," Scripta Met., 15, 1981, 633-636.

39. S. Suresh and R. O. Ritchie, "A Geometric Model for Fatigue Crack Closure Induced by Fracture Surface Roughness," Metall. Trans. A, 13A, 1982, 1627-1631.

40. G. T. Gray, III, J. C. Williams and A. W. Thompson, "Roughness-Induced Crack Closure: An Explanation for Microstructurally Sensitive Fatigue Crack Growth," Metall. Trans. A, 14A, 1983, 421-433.

41. R. O. Ritchie, "Fatigue Crack Growth: Mechanics and Fatigue Mechanisms," in the Encyclopedia of Materials Science and Engineering, ed. by M. B. Bever, Pergamon Press, Oxford and New York, 1983, in press.

42. S. Newman, "Kinetics of Wetting of Surfaces by Polymers: Capillary Flow," J. Colloid Interface Sci., 26, 1968, 209-213.

43. S. Suresh, "Mechanisms of Environmentally-Influenced Corrosion Fatigue Crack Growth in Lower Strength Steels," Sc.D. Thesis, M.I.T., 1981.

44. A. N. Carlson, Jr., Fisher Scientific Company, Fair Lawn, New Jersey, private communication.

45. J. E. Srawley, "Wide Range Stress Intensity Factor Expressions for ASTM E 399 Standard Fracture Toughness Specimens," Int. J. Fract., 12, 1976, 475-476.

46. R. O. Ritchie, G. G. Garrett and J. F. Knott, "Crack-Growth Monitoring: Optimisation of the Electrical Potential Technique Using an Analogue Method," Int. J. Fract. Mech., 7, 1971, 462-467.

47. R. O. Ritchie, "Crack Growth Monitoring: Some Consideration on the Electrical Potential Method," Dept. of Metallurgy and Materials Science Report, Univ. of Cambridge, January 1972.

48. R. P. Skelton and J. R. Haigh, "Fatigue Crack Growth Rates and Thresholds in Steels under Oxidising Conditions," Mat. Sci. Eng., 36, 1978, 17-25.

49. L. K. L. Tu and B. B. Seth, "Threshold Corrosion Fatigue Crack Growth in Steels," J. Test. Eval., 6, 1978, 66-74.

50. G. E. Nordmark and W. G. Fricke, "Fatigue Crack Arrest at Low Stress Intensities in a Corrosive Environment," J. Test. Eval., 6, 301-303.

51. R. Brazill, G. W. Simmons and R. P. Wei, "Fatigue Crack Growth in 2¼Cr-1Mo Steel Exposed to Hydrogen Containing Gases," J. Eng. Mat. Tech., Trans. ASME, Series H, 101, 1979, 199-204.

52. W. L. Holshouser and H. P. Utech, "Effect of Oleophobic Films on Fatigue Crack Propagation," Proc. ASTM, 61, 1961, 749-756.

53. A. Hartman, "On the Effect of Oxygen and Water Vapor on the Propagation of Fatigue Cracks in 2024-T3 Alclad Sheet," Int. J. Fract. Mech., 1, 1965, 167-188.

54. F. J. Bradshaw and C. Wheeler, "The Effect of Environment on Fatigue Crack Growth in Aluminum and Some Aluminum Alloys," Appl. Mat. Res., 5, 1966, 112-120.

55. K. Endo, K. Komai and O. Furukawa, "The Effects of Atmosphere on Fatigue Crack Propagation," Bull. JSME, 10, 1967, 581-587.

56. P. Lukás, L. Kunz and J. Bartos, "Influence of the Gaseous Environments on Fatigue Crack Propagation in an Austenitic Steel," Mat. Sci. Eng., 56, 1982, 11-18.

57. I. M. Austen and P. McIntyre, "Corrosion Fatigue of High-Strength Steel in Low-Pressure Hydrogen Gas," Met. Sci., 13, 1979, 420-428.

58. P. Smith and A. T. Steward, "Effect of Aqueous and Hydrogen Environments on Fatigue Crack Growth in 2Ni-Cr-Mo-V Rotor Steel," Met. Sci., 13, 429-435.

59. I. S. Enochs and O. F. Devereux, "Fatigue Crack Growth in 5052-H34 Aluminum in Vacuum and Active Gas Environments," Metall. Trans. A, 6A, 1975, 391-397.

60. R. P. Wei, P. S. Pao, R. G. Hart, T. W. Weir and G. W. Simmons, "Fracture Mechanics and Surface Chemistry Studies of Fatigue Crack Growth," Metall. Trans. A, 11A, 1980, 151-158.

61. P. K. Liaw, T. R. Leax, R. S. Williams and M. G. Peck, "Influence of Oxide-Induced Crack Closure on Near-Threshold Fatigue Crack Growth Behavior," Acta Met., 30, 1982, 2071-2078.

62. A. K. Vasudévan and S. Suresh, "Influence of Corrosion Deposits on Near-Threshold Fatigue Crack Growth Behavior in 2XXX and 7XXX Series Aluminum Alloys," Metall. Trans. A, 13A, 1982, 2271-2280.

63. S. Suresh, I. G. Palmer and R. E. Lewis, "The Effect of Environment on Fatigue Crack Growth Behavior of 2021 Aluminum Alloy," Fat. Eng. Mat. Struct., 5, 1982, 133-150.

64. D. D. Fuller, in Theory and Practice of Lubrication for Engineers, John Wiley & Sons, New York, 1956, 134-135.

65. A. Turnbull, "A Theoretical Evaluation of the Influence of Mechanical Variables on the Concentration of Oxygen in a Corrosion Fatigue Crack," Corrosion Sci., 22, 1982, 877-893.

66. C. C. Veerman and T. Muller, "The Location of the Apparent Rotation Axis in Notched Bend Testing," Eng. Fract. Mech., 4, 1972, 25-32.

67. G. C. Sih, in Handbook of Stress-Intensity Factors, Lehigh University, Bethlehem, Pennsylvania, 1973.

68. J. Landes and D. McCabe, Westinghouse R & D Center, Pittsburgh, PA, private communication.

69. D. E. Swets and R. C. Frank, "Hydrogen from a Hydrocarbon Lubricant Absorbed by Ball Bearings," Trans. the Metall. Soc. AIME, 221, 1961, 1082-1083.

70. C. M. Branco, J. C. Radon and C. E. Culver, "Influence of Specimen Orientation and Loading History on S.C.C. in an Aluminum Alloy," Corrosion Sci., 17, 1977, 125-141.

APPENDIX

A. Determination of the Resultant Hydrodynamic Force within a Closing Fatigue Crack *Partially* Penetrated by a Viscous Fluid

The expression of the hydrodynamic pressure distribution due to the partial penetration of viscous fluid into a closing fatigue crack (Fig. 18a) has been given by [64]:

$$p(x) = -\frac{6\eta\rho v x}{H^3}(x - d) \tag{11}$$

where η = kinematic viscosity

ρ = density of fluid

v = approaching velocity of the crack walls in m/sec

d = penetration distance

H = average crack opening displacement

The resultant force (per unit thickness) can be obtained by integrating Eq. 11 with respect to x from x = 0 to x = d:

$$F_p^e = \int_0^d p(x)dx = -\int_0^d \frac{6\eta\rho v x}{H^3}(x - d)dx$$

$$= \frac{\eta\rho v d^3}{H^3} \tag{21}$$

Assume the angle θ between the crack faces is small and the crack walls approach at a constant velocity which is conservatively estimated as the product of the length measured from the crack mouth to the plastic hinge point (= a + rb) and the angular closing velocity (= $d\theta/dt$), i.e.,

$$v \sim (a + rb)\frac{d\theta}{dt} \sim (a + rb)\frac{\Delta\theta}{\Delta t} \tag{22}$$

Since $\theta \sim \frac{h}{a + rb}$ and $h = \frac{a + rb}{rb}\delta$ (Eq. 8), therefore $\theta = \frac{\delta}{rb}$ and hence

$$\Delta\theta = \frac{\Delta\delta}{rb} \tag{23}$$

Taking $\Delta\delta = 0.49\,\frac{\Delta K^2}{2YE}$ [1], the approaching velocity of the crack walls during the unloading half cycles ($\Delta t = 1/2f$) is thus approximately

$$v \sim \frac{f(a + rb)\Delta K^2}{2YErb} \tag{24}$$

where f is frequency. The average crack opening displacement at minimum load (or K_{min}) based on Eqs. 5 and 8 is estimated as

$$\begin{aligned} H_{min} &= \tfrac{1}{2}(h_{min} + \delta_{min}) \\ &= \tfrac{1}{2}(2 + \tfrac{a}{rb})\,\frac{K^2}{YE}\left(\frac{R}{1 - R}\right)^2 \qquad \left(\because K_{min} = \frac{R}{1 - R}\Delta K\right) \end{aligned} \tag{25}$$

Consequently, the resultant hydrodynamic force (per unit thickness) when externally applied load reaches its minimum value (or K_{min}) can be obtained by substituting Eqs. 24 and 25 into Eq. 21 as

$$F_p^e = 3.2 \times 10^{-8}\,\eta\rho f d^3\,\frac{a + rb}{(a + 2rb)^3}\left(\frac{YErb}{\Delta K^2}\right)^2\left(\frac{1 - R}{R}\right)^6 \tag{11}$$

B. Determination of the Resultant Hydrodynamic Force Within a Closing Fatigue Crack *Fully* Penetrated by a Viscous Fluid

The expression of the hydrodynamic pressure distribution due to the fully penetration of viscous fluid into a closing fatigue crack (Fig. 16a) has been given by Endo et al. [5]:

$$p(x) = \frac{6\eta\rho a^3}{h^3}\frac{d\theta}{dt}\log(1 - \frac{x}{a}) = P_f^e \log(1 - \frac{x}{a}) \tag{2}$$

where h = crack mouth opening displacement

$d\theta/dt$ = angular closing velocity of crack walls in sec^{-1}

a = crack length

The resultant force (per unit thickness) F_f^e can be obtained by integrating Eq. 2 with respect to x from x = 0 to x = a, thus

$$F_f^e = \int_0^a p(x)dx = \frac{6\eta\rho a^4}{h^3}\frac{d\theta}{dt} \tag{26}$$

$$= aP_f^e$$

From Eqs. 22 and 24, we get

$$\frac{d\theta}{dt} \sim \frac{\Delta\theta}{\Delta t} = \frac{v}{a + rb} = \frac{f\Delta K^2}{2YErb} \tag{27}$$

Since $h_{min} = \frac{a + rb}{rb}\delta_{min}$ (Fig. 8) and $\delta_{min} = 0.49\ K_{min}^2/YE$, the resultant force becomes

$$F_f^e = 1.1 \times 10^{-8}\ \eta\rho f(\frac{1}{a + rb})^3(\frac{a^2YErb}{\Delta K^2})^2(\frac{1 - R}{R}) \tag{28}$$

$$= aP_f^e$$

$$\Rightarrow \quad P_f^e = 1.1 \times 10^{-8}\, \eta\rho f \left(\frac{a}{a + rb}\right)^3 \left(\frac{YErb}{\Delta K^2}\right)^2 \left(\frac{1 - R}{R}\right)^6 \tag{17}$$

Table I. Base plate chemistries of SA542-3 steel (wt. pct.).

C	Mn	Si	Ni	Cr	Mo	Cu	P	S
0.12	0.45	0.21	0.11	2.28	1.05	0.12	0.014	0.015

Table II. As-received heat treatment of SA542-3 steel.

Treatment	Time and Temperature
Austenitize	5½ hrs at 954°C
Water Quench	
Temper	8 hrs at 663°C
Stress Relieve	15 hrs at 593°C
	22 hrs at 649°C
	18 hrs at 663°C

Table III. Ambient temperature mechanical properties of SA542-3 steel (¼ to ½T sections).

Strength (MPa)	U.T.S. (MPa)	Elongation (%)	Reduction in Area (%)	Charpy Impact Energy (J)	K_{IC} (MPa$\sqrt{m}$)	K_{ISCC} (MPa$\sqrt{m}$)
496±7	610±17	25	77	197±18	295	85

Table IV. Relevant ambient temperature physical properties of silicone and paraffin oils.

Oil	Kinematic Viscosity (cS)	Density (gm/cm^3)	Surface Tension (dyne/cm)
Silicone Oil	5	0.92	19.7
	1,000	0.971	21.2
	12,500	0.975	21.5
	60,000	0.975	21.5
Paraffin Oil	25	0.87	35.0
	75	0.89	36.0

Table V. Experimental fatigue threshold data for SA542-3 steel tested in oil environments at R = 0.05 and 0.75 (50 Hz sine wave).

Oil Environment	Kinematic Viscosity (cS)	Load Ratio R	Threshold Stress Intensity ΔK_0 (MPa$\sqrt{m}$)
Silicone Oil	5	0.05	6.4
	1,000	"	6.1
	12,500	"	5.8
	60,000	"	5.7
Paraffin Oil	25	"	5.9
	75	"	5.2
Silicone Oil	5	0.75	2.8
	1,000	"	3.0
	12,500	"	3.0
	60,000	"	3.0
Paraffin Oil	25	"	3.0

Table VI. Predicted closure stress intensities K_{cl}^{w} and the effective stress intensity ranges ΔK_{eff} using proposed viscous fluid-induced crack closure model (Eq. 15). Calculations are performed for SA542-3 steel at a crack length of a = 25 mm and an applied (nominal) stress intensity range of $\Delta K = 10$ MPa$\sqrt{m}$ in oil environments at both R = 0.05 and 0.75[1].

Oil Environment	Kinematic Viscosity η (cS)	Load Ratio R	Penetration Depth d_{eff} (mm)	Stress Intensity Increment Due to Hydrodynamic Pressure K_p^c (MPa$\sqrt{m}$)	Closure Stress Intensity K_{cl}^{w} (MPa$\sqrt{m}$)	Effective Stress Intensity Range ΔK_{eff} (MPa$\sqrt{m}$)
Silicone Oil	5	0.05	0.02	2.5	3.0	7.5
	1,000	"	0.001	0.3	0.8	9.7
	12,500	"	0.0004	0.05	~0.6	~10.0
	60,000	"	0.0002	0.03	~0.6	~10.0
Paraffin Oil	25	"	0.01	2.6	3.1	7.4
	75	"	0.01	1.6	2.1	8.4
Silicone Oil	5	0.75	0.1	-	30[2]	10[3]
	1,000	"	0.005	-	30[2]	10[3]
	60,000	"	0.001	-	30[2]	10[3]
Paraffin Oil	25	"	0.05	-	30[2]	10[3]

(1) Calculations based on the following assumptions:

(a) Compact tension specimen.
(b) Crack length a = 25 mm (initial crack length a_o = 17.5 mm).
(c) Nominal applied stress intensity range $\Delta K = 10$ MPa$\sqrt{m}$.

(2) K_p^c is negligible $\Rightarrow K_{cl}^{w} = (K_{min})_{eff} = K_{min}$.

(3) No closure: $\Delta K_{eff} = \Delta K$.

Table VII. Comparison of quantitative extent of viscous fluid-induced crack closure (VICC) based on current partial penetration model (Table VI) and Endo et al.'s full penetration model[1]

Oil Environment	Kinematic Viscosity η (cS)	Load Ratio R	Endo et al.'s Model K^w_{cl} (MPa$\sqrt{m}$)	Present Model K^w_{cl} (MPa$\sqrt{m}$)
Silicone Oil	5	0.05	9.37×10^8	3.0
	1,000	"	1.98×10^{11}	0.8
	12,500	"	2.48×10^{12}	0.6
	60,000	"	1.19×10^{13}	0.6
Paraffin Oil	25	"	4.43×10^9	3.1
	75	"	1.36×10^{10}	2.1
Silicone Oil	5	0.75	30.0[2]	30[2]
	1,000	"	35.8	30[2]
	60,000	"	377.4	30[2]
Paraffin Oil	25	"	30.1	30[2]

[1] Calculations based on the following assumptions:

(a) Compact tension specimen
(b) Crack length a = 25 mm (initial crack length a_0 = 17.5 mm)
(c) Nominal applied stress intensity range $\Delta K = 10$ MPa$\sqrt{m}$

[2] Closure is negligible $\Rightarrow K^w_{cl} = (K_{min})_{eff} = K_{min}$

Table VIII. Characteristics of fatigue crack growth in SA542-3 steel tested in dry oil environments at intermediate and near-threshold growth rates.

Variables	Intermediate Growth Rates ($\geq 10^{-6}$ mm/cycle)		Near-Threshold Growth Rates ($\leq 10^{-6}$ mm/cycle)	
	R = 0.05	R = 0.75	R = 0.05	R = 0.75
Influence of oil environments	$(da/dN)_{oil} < (da/dN)_{moist\ air}$		$(da/dN)_{oil} > (da/dN)_{moist\ air}$ ⇒ $(\Delta K_o)_{oil} < (\Delta K_o)_{air}$	$(da/dN)_{oil} = (da/dN)_{moist\ air}$ ⇒ $(\Delta K_o)_{oil} = (\Delta K_o)_{air}$
Influence of oil viscosity (η)	$(da/dN)_{high\ \eta} > (da/dN)_{low\ \eta}$	No effect of η	Small and finite trend of increasing da/dN (or decreasing ΔK_o) with increasing η	No effect of η
Influence of type of oil	$(da/dN)_{silicone\ oil} > (da/dN)_{paraffin\ oil}$	$(da/dN)_{silicone\ oil} < (da/dN)_{paraffin\ oil}$	$(da/dN)_{silicone\ oil} = (da/dN)_{paraffin\ oil}$	No effect of type of oil
Influence of load ratio (R) on da/dN in oil environments	1. $(da/dN)_{R = 0.05} < (da/dN)_{R = 0.75}$ 2. Much more significant at near-threshold growth rates			
Fractographic characteristics in oil environments	Predominantly intergranular		Predominantly transgranular	
Reasons responsible for differences in growth rates (between oils and moist air)	Exclusion of moisture from crack tip region by oil environments ⇒ minimization of conventional corrosion fatigue processes (H_2 embrittlement)		Minimization of oxide-induced crack closure	--
Reasons responsible for different growth rates in various oil environments	Hydrodynamic wedging effects due to oil penetration into the crack	Probable H_2 embrittlement due to unexpected decomposition of paraffin oils' hydrocarbon constituents	--	--

Table IX

SCHEME FOR ΔK_{eff} COMPUTATIONS

Partial Penetration Model

(1) $K = K_\infty - K_p = K_\infty - \dfrac{2QF_p}{\sqrt{\pi a}}$

(2) $F_p = \dfrac{\eta\rho\dot{H}d^3}{H^3}$

(3) $H = \dfrac{K^2}{4\sigma_y E}\left(\dfrac{a - a_o + 2rb}{rb}\right)$

(4) $K_\infty = K_m + \dfrac{\Delta K}{2}\sin wt$

(5) $d = \left[\dfrac{\gamma_L \cos\beta}{3\eta\rho}\int_0^t H dt\right]^{\frac{1}{2}}$

From Eqns. (1)-(5)

$$\Rightarrow \boxed{\lambda \frac{\dot{K}}{K^5} + K = K_m + \frac{\Delta K}{2}\sin wt}$$

where $\lambda = \dfrac{64Q\eta\rho d^3}{\sqrt{\pi a}}\left(\dfrac{\sigma_y Erb}{a - a_o + 2rb}\right)^2$

Full Penetration Model

(1) $K = K_\infty - K_p = K_\infty - \dfrac{2Q'F_f}{\sqrt{\pi a}}$

(2) $F_f = \dfrac{6\eta\rho(a - a_o)^4}{h^3}\cdot\dfrac{d\theta}{dt}$

(3) $\dfrac{d\theta}{dt} \approx \dfrac{\Delta\theta}{\Delta t} \approx \dfrac{a - a_o + 2rb}{a - a_o + rb}\cdot\dfrac{K\dot{K}}{\sigma_y Erb}$

(4) $K_\infty = K_m + \dfrac{\Delta K}{2}\sin wt$

From Eqns. (1)-(4)

$$\Rightarrow \boxed{\lambda' \frac{\dot{K}}{K^5} + K = K_m + \frac{\Delta K}{2}\sin wt}$$

where $\lambda' = \dfrac{96Q'\eta\rho(a - a_o)^4(\sigma_y Erb)^2(a - a_o + 2rb)}{(a - a_o + rb)^4\sqrt{\pi a}}$

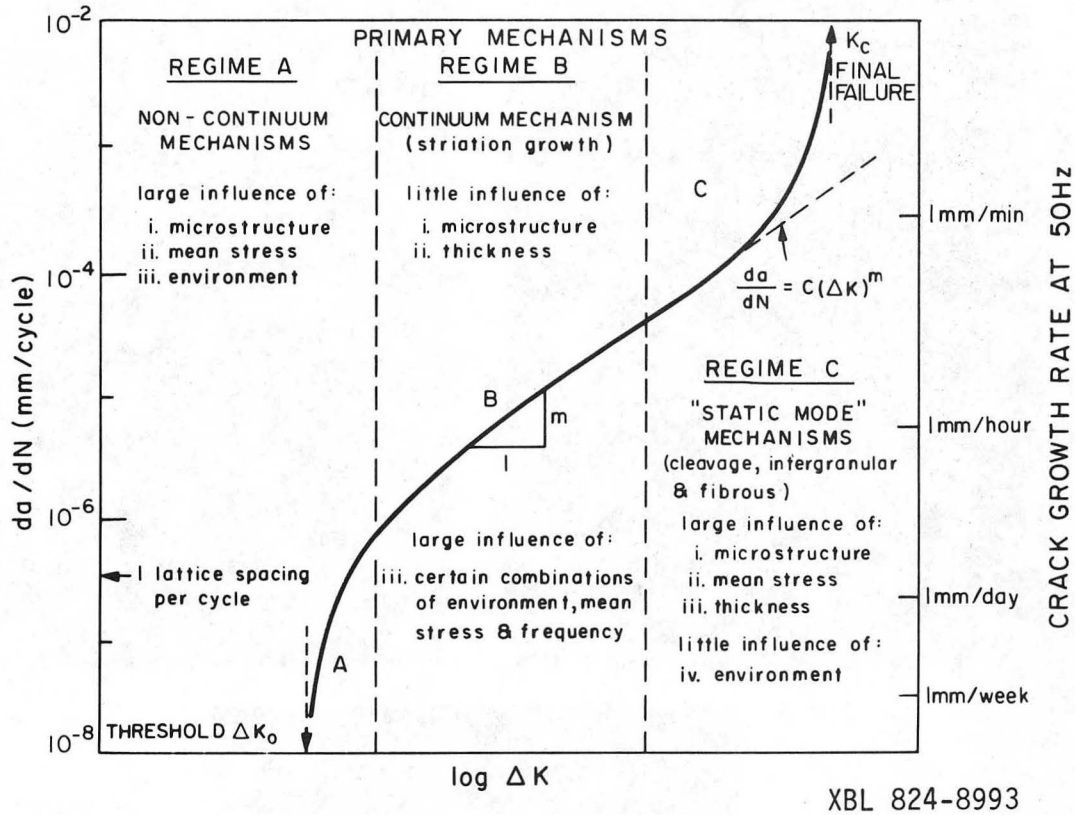

Fig. 1. Schematic variation of fatigue crack propagation rate (da/dN) with stress intensity range (ΔK), showing regimes of primary growth rate mechanisms. ΔK_o is the threshold stress intensity for crack growth and K_c the stress intensity at final failure [1].

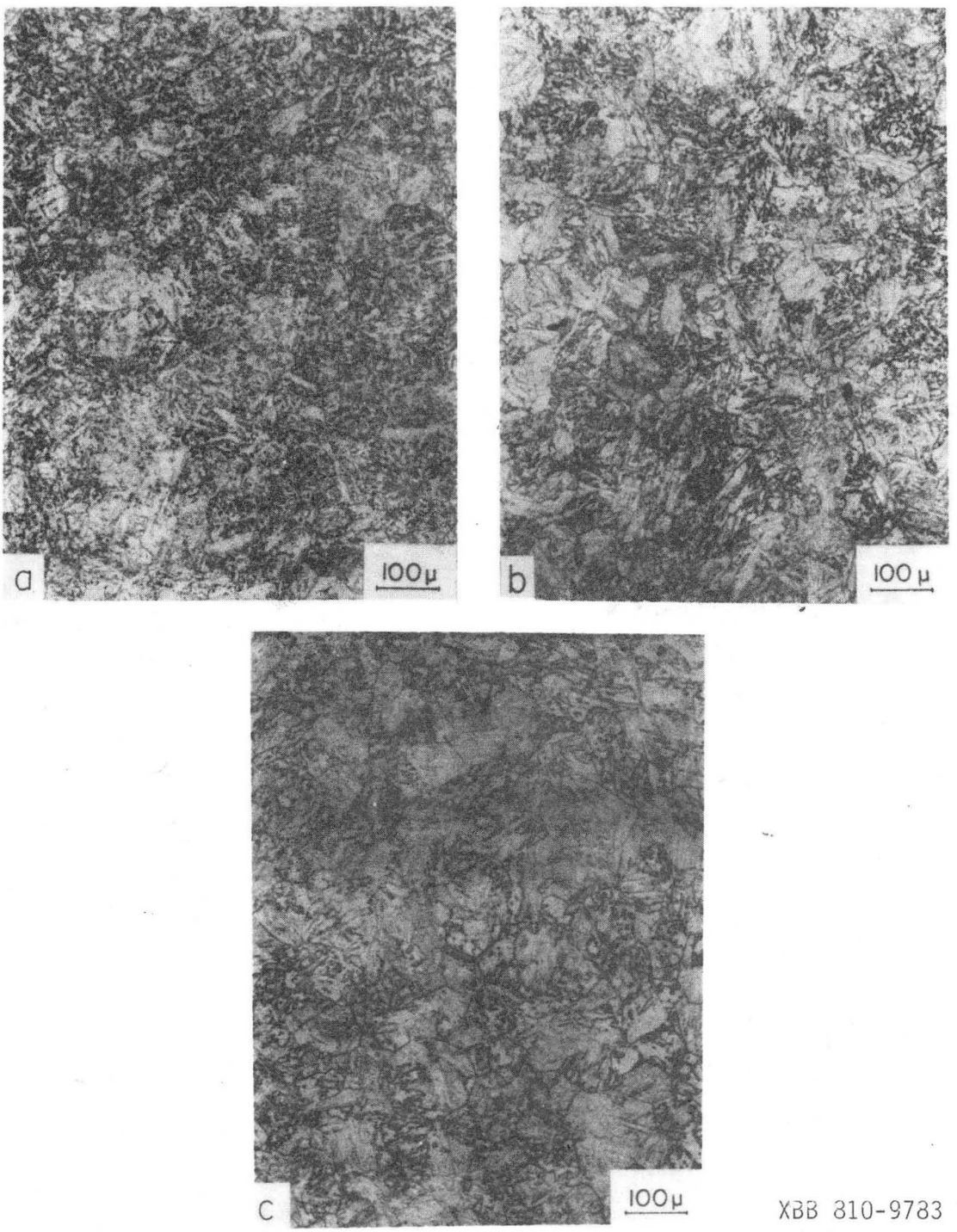

Fig. 2. Optical micrograph of SA542-3 steel, 174 mm thick base plate at (a) surface, (b) quarter thickness ($\frac{1}{4}$T), and (c) mid-thickness ($\frac{1}{2}$T) locations.

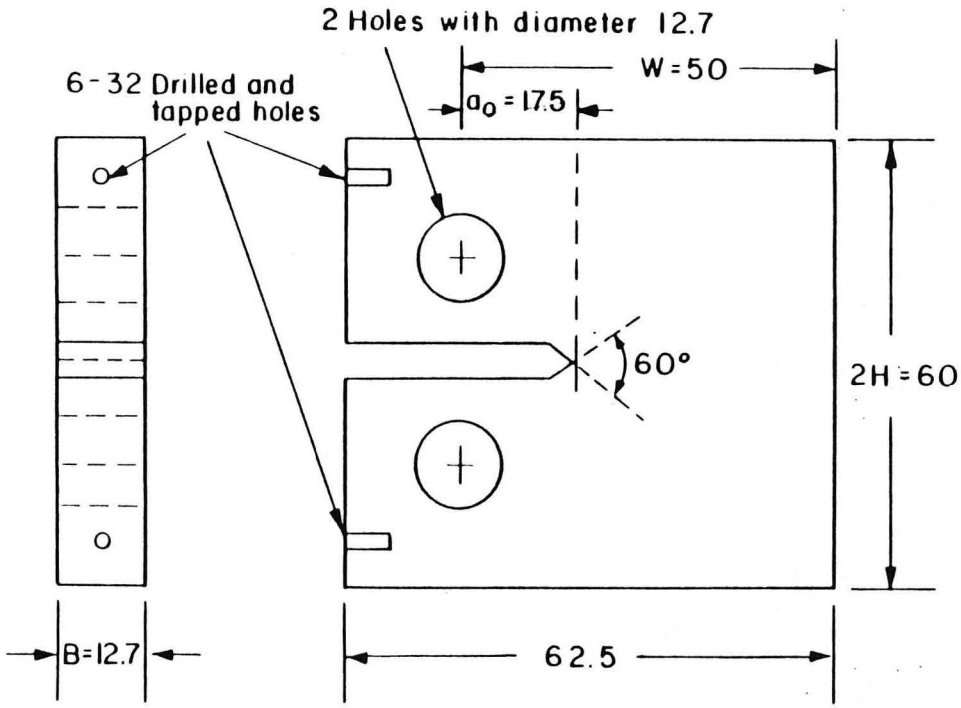

All dimensions in mm

Compact (CT) fatigue testpiece

H/W = 0.60

B = 12.7 mm (0.50 in)

W = 50 mm (1.97 in)

a_0/W = 0.35

$$K = \frac{P}{BW^{1/2}} \cdot \frac{(2+\alpha)}{(1-\alpha)^{3/2}} \left(0.886 + 4.64\alpha - 13.32\alpha^2 + 14.72\alpha^3 - 5.6\alpha^4\right) \text{ where } \alpha = a/W$$

XBL 835-9516

Fig. 3. Design of compact tension specimen used for fatigue crack propagation tests.

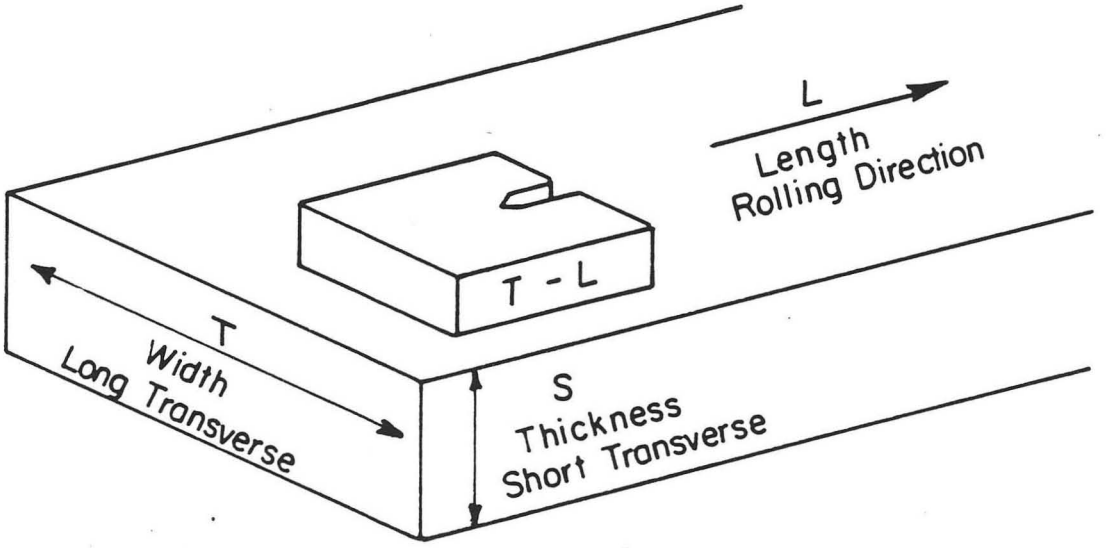

XBL 832-5305

Fig. 4. Crack plane orientation of the compact tension specimen machined from base plates.

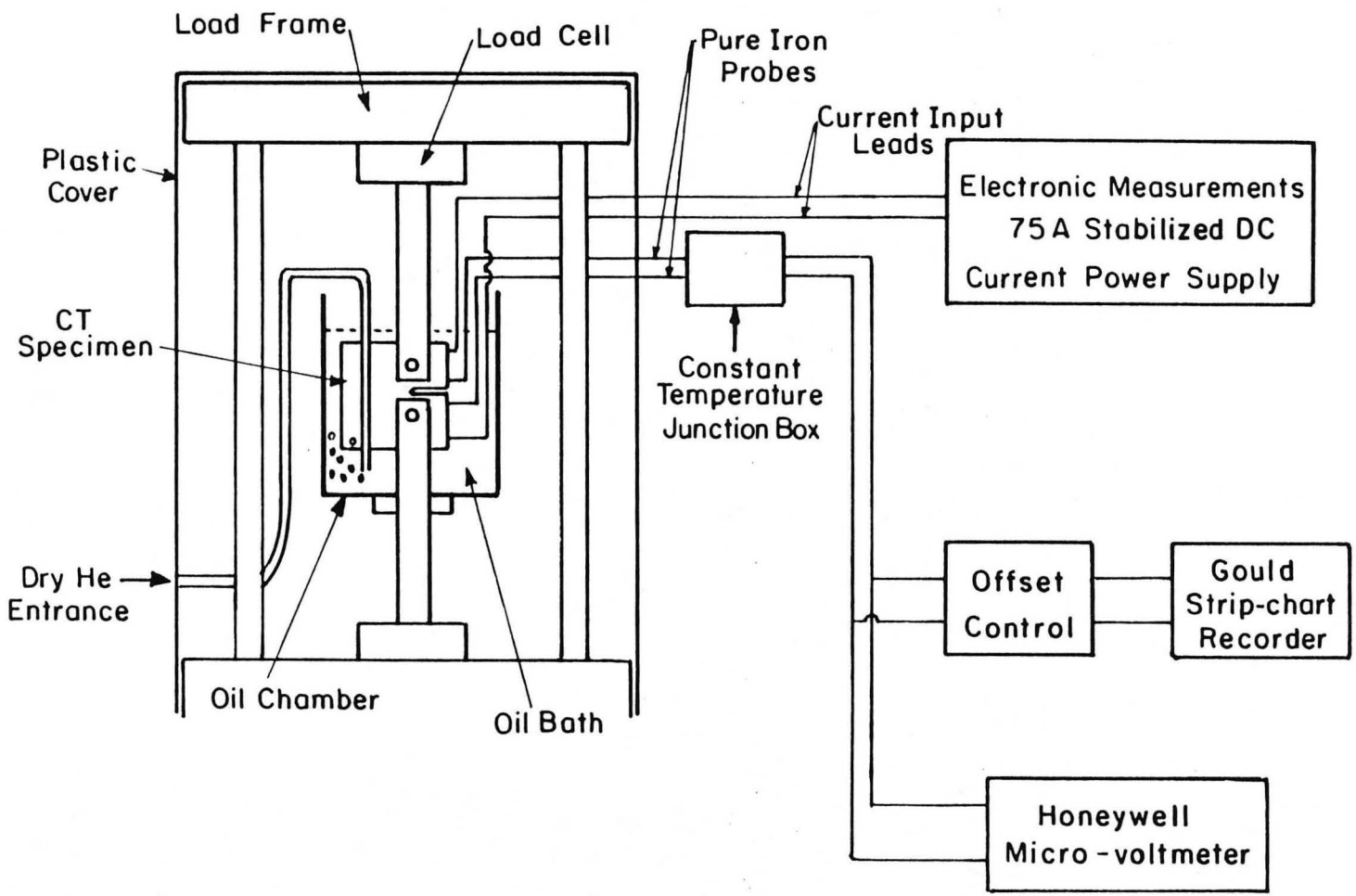

XBL 832-5299

Fig. 5. Experimental set-up for fatigue tests in oil environments and electrical potential crack monitoring system.

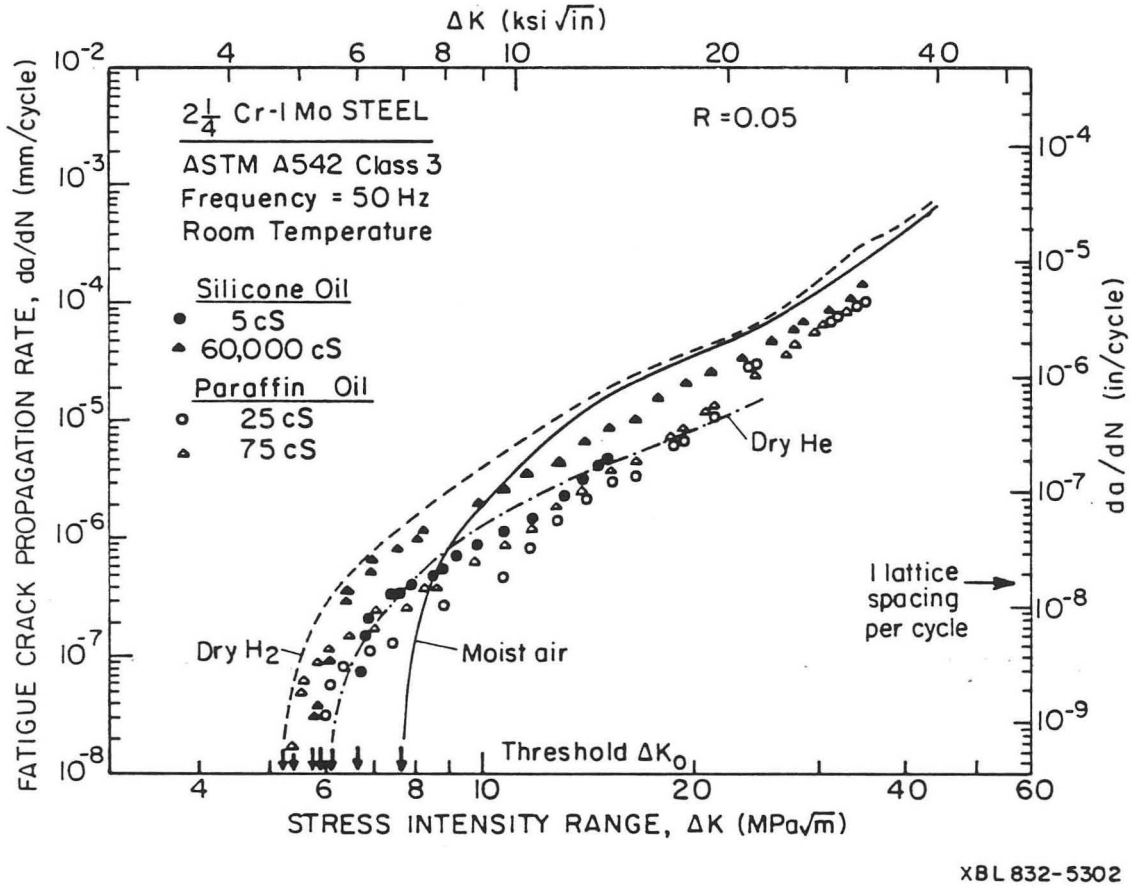

Fig. 6. Fatigue crack propagation in SA542-3 steel tested at R = 0.05 (50 Hz) in oil environments (data points), moist air, dry hydrogen gas (data curves) [32].

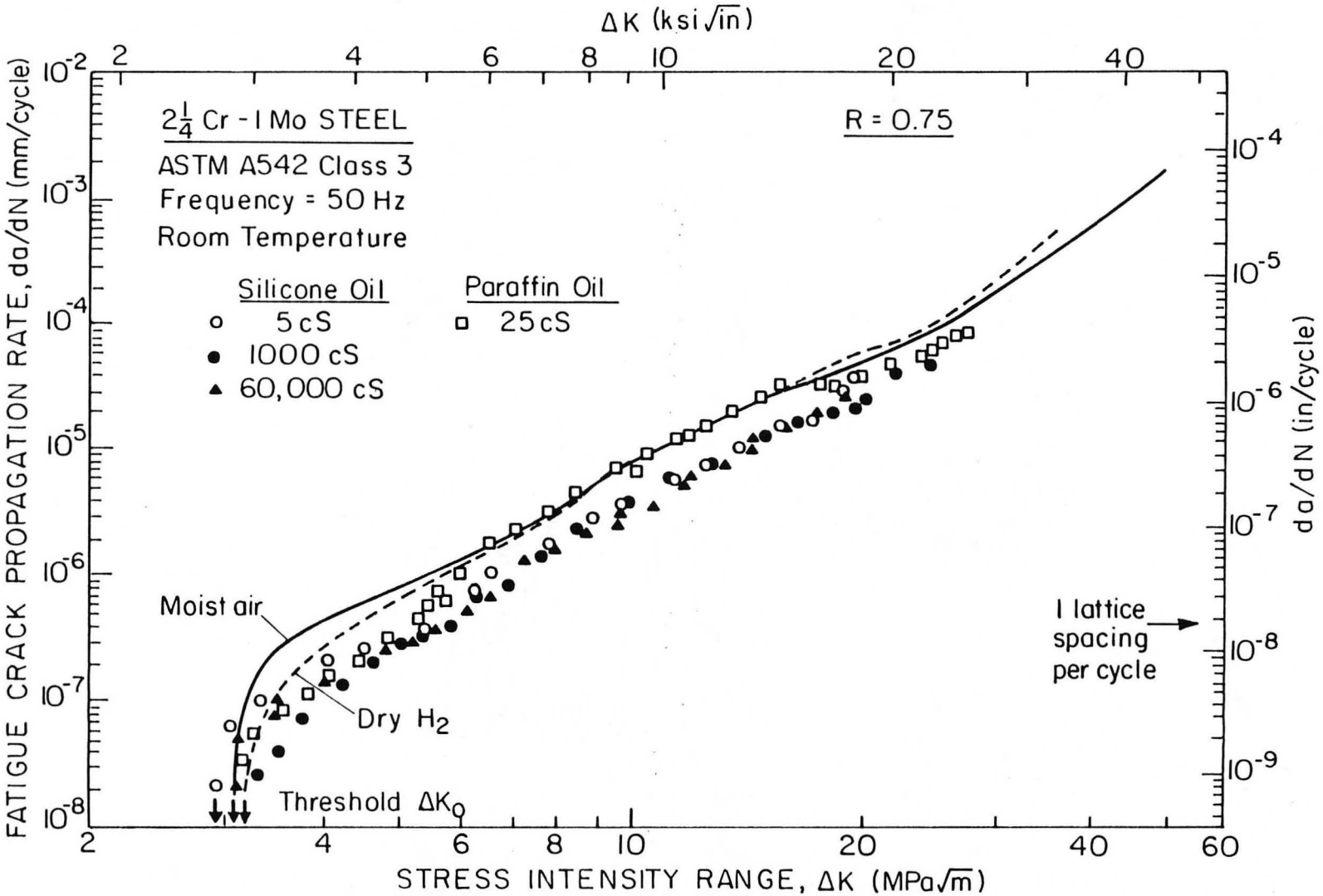

Fig. 7. Fatigue crack propagation in SA542-3 steel tested at R = 0.75 (50 Hz) in oil environments (data points), moist air, dry hydrogen gas (data curves) [32].

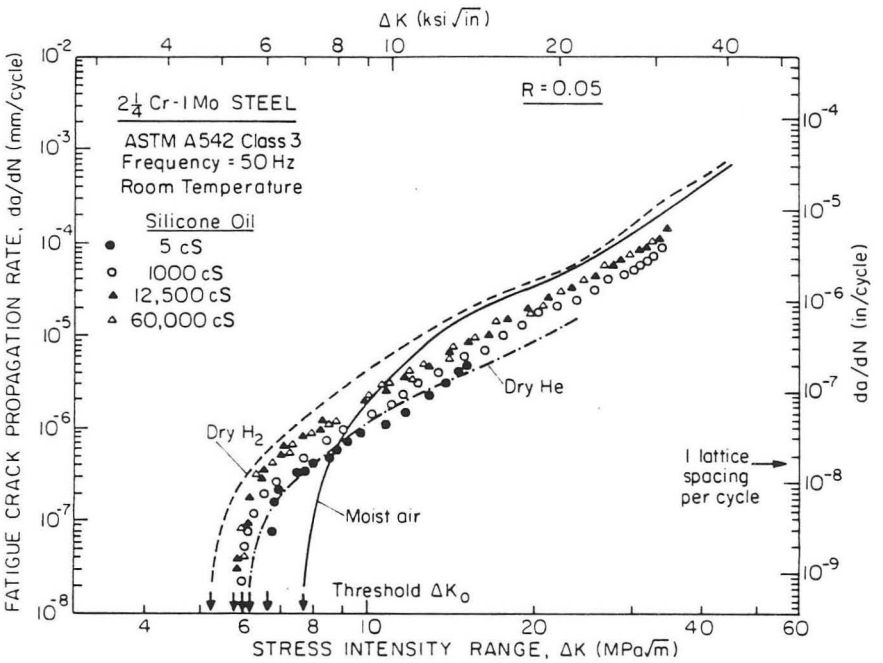

(a)

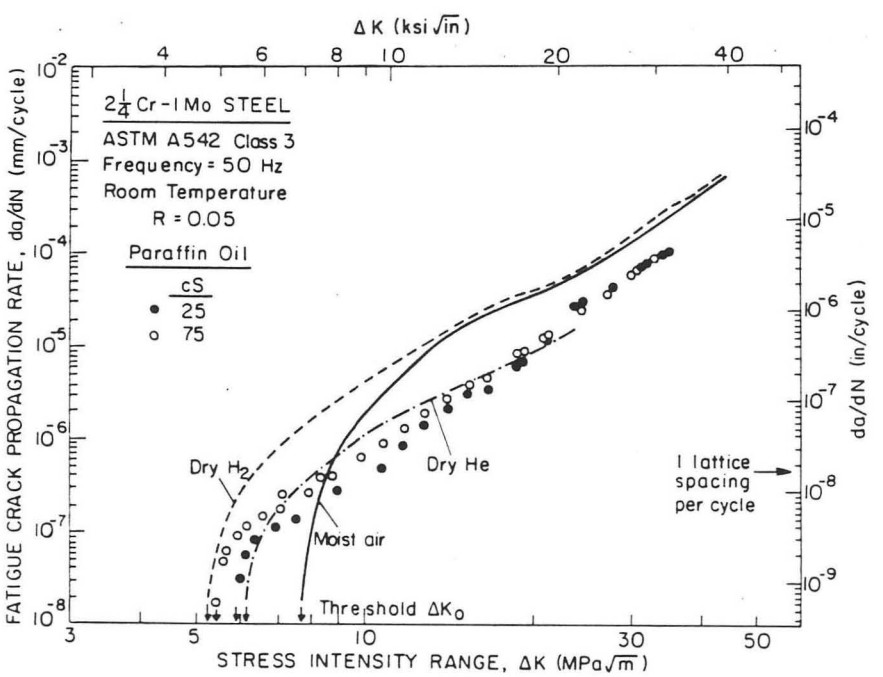

(b)

XBL 832-5311

Fig. 8. Fatigue crack propagation in SA542-3 steel tested at R = 0.05 in (a) silicone oils and (b) paraffin oils.

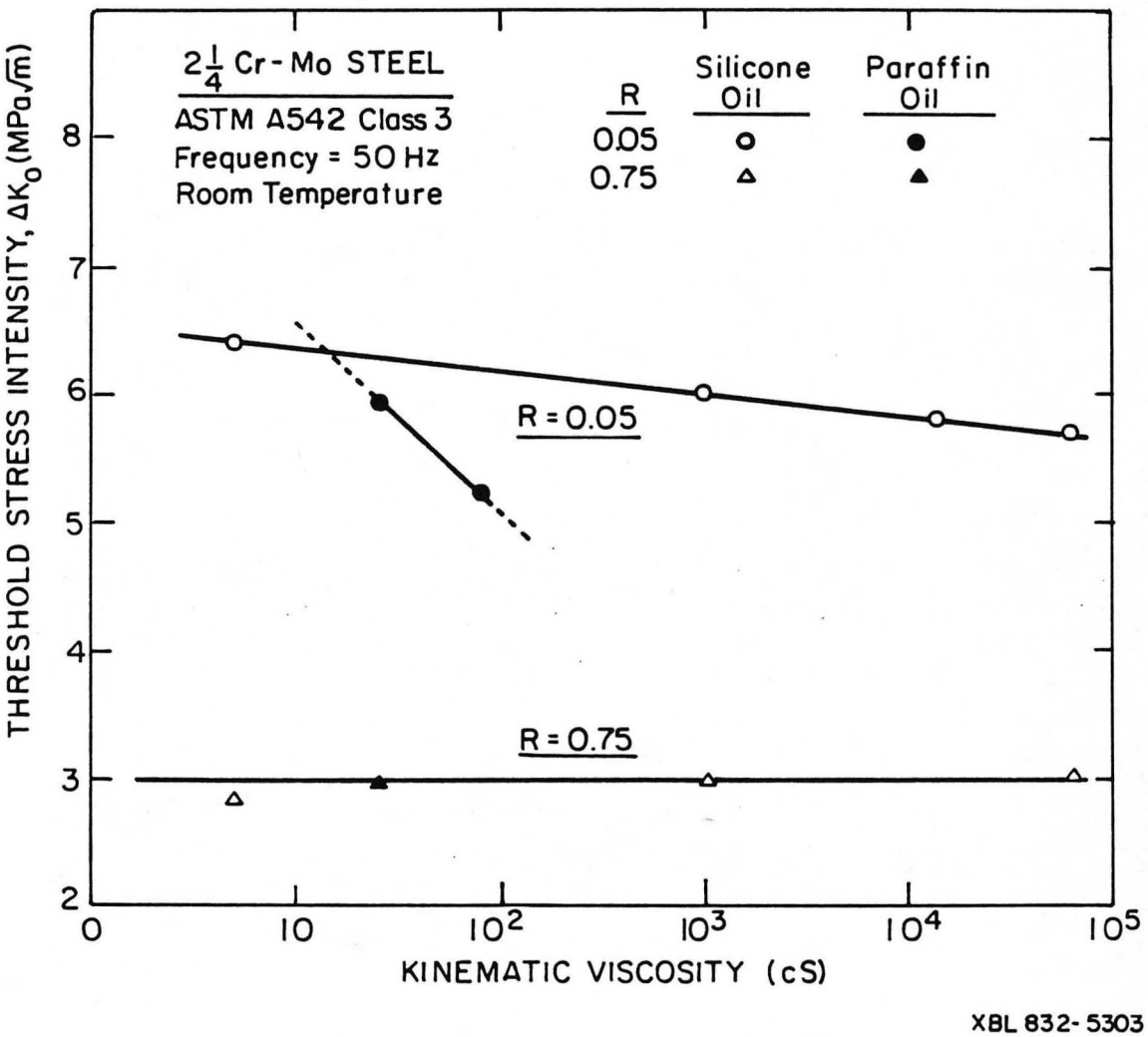

Fig. 9. Variation of threshold stress intensity of SA542-3 steel tested at R = 0.05 and 0.75 (50 Hz) with the kinematic viscosity of oil environments.

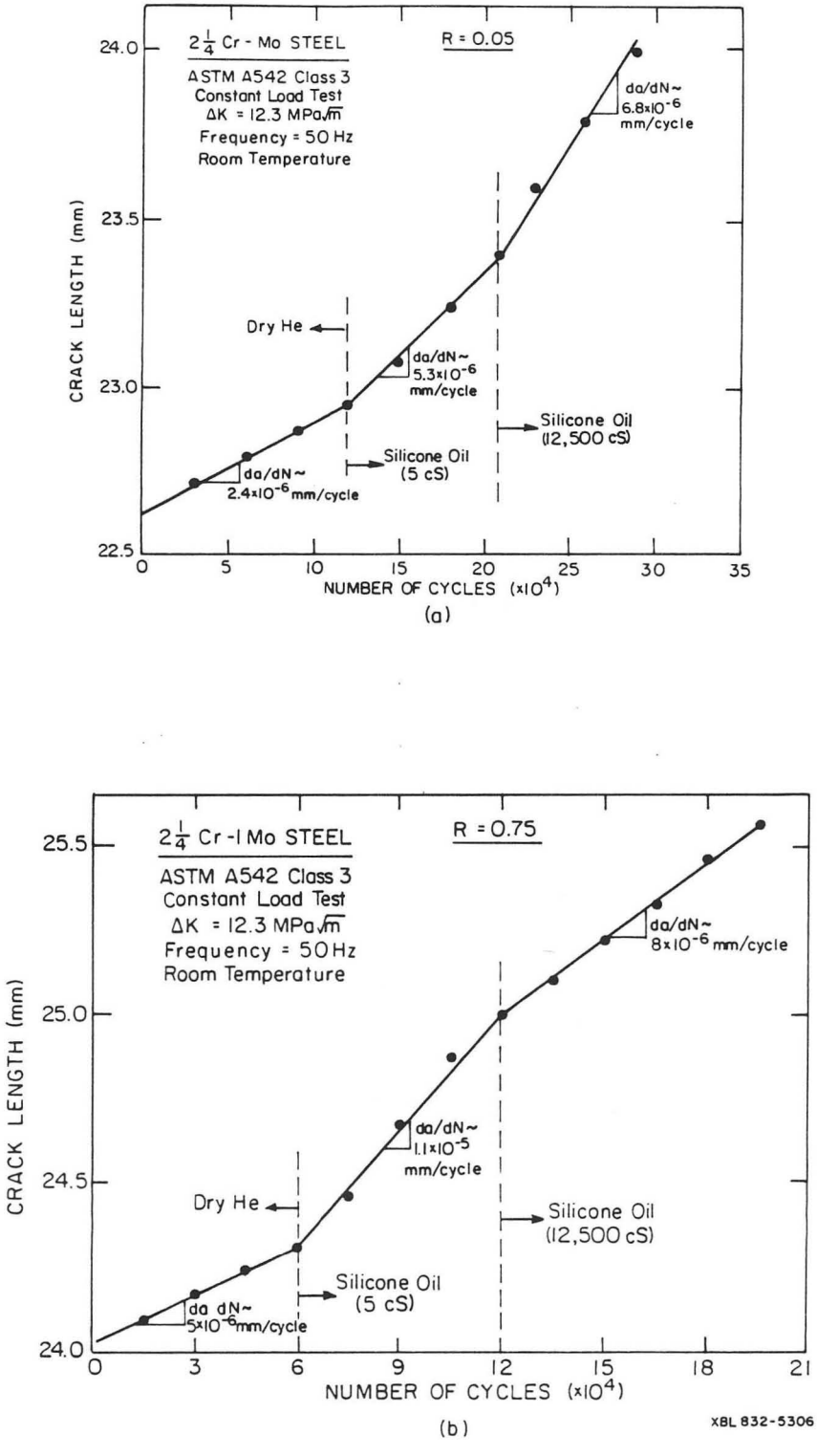

Fig. 10. Fatigue crack growth in SA542-3 steel tested at a constant stress intensity of about 12.3 MPa$\sqrt{m}$ at (a) R = 0.05, and (b) 0.75, showing the effects of environment and oil viscosity at different load ratios.

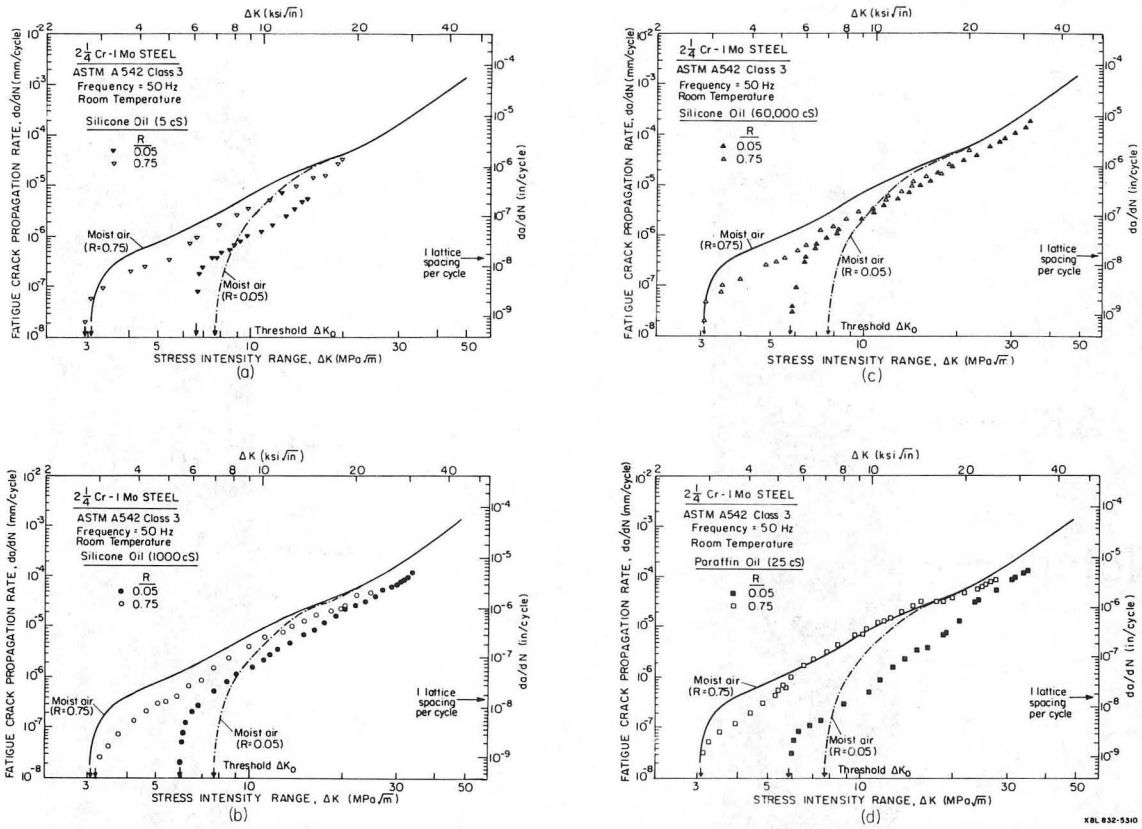

Fig. 11. Fatigue crack propagation in SA542-3 steel tested at R = 0.05 and 0.75 (50 Hz) in (a) 5 cS, (b) 1000 cS, (c) 60,000 cS silicone oils, and (d) 25 cS paraffin oil, showing the effect of load ratio in various oil environments.

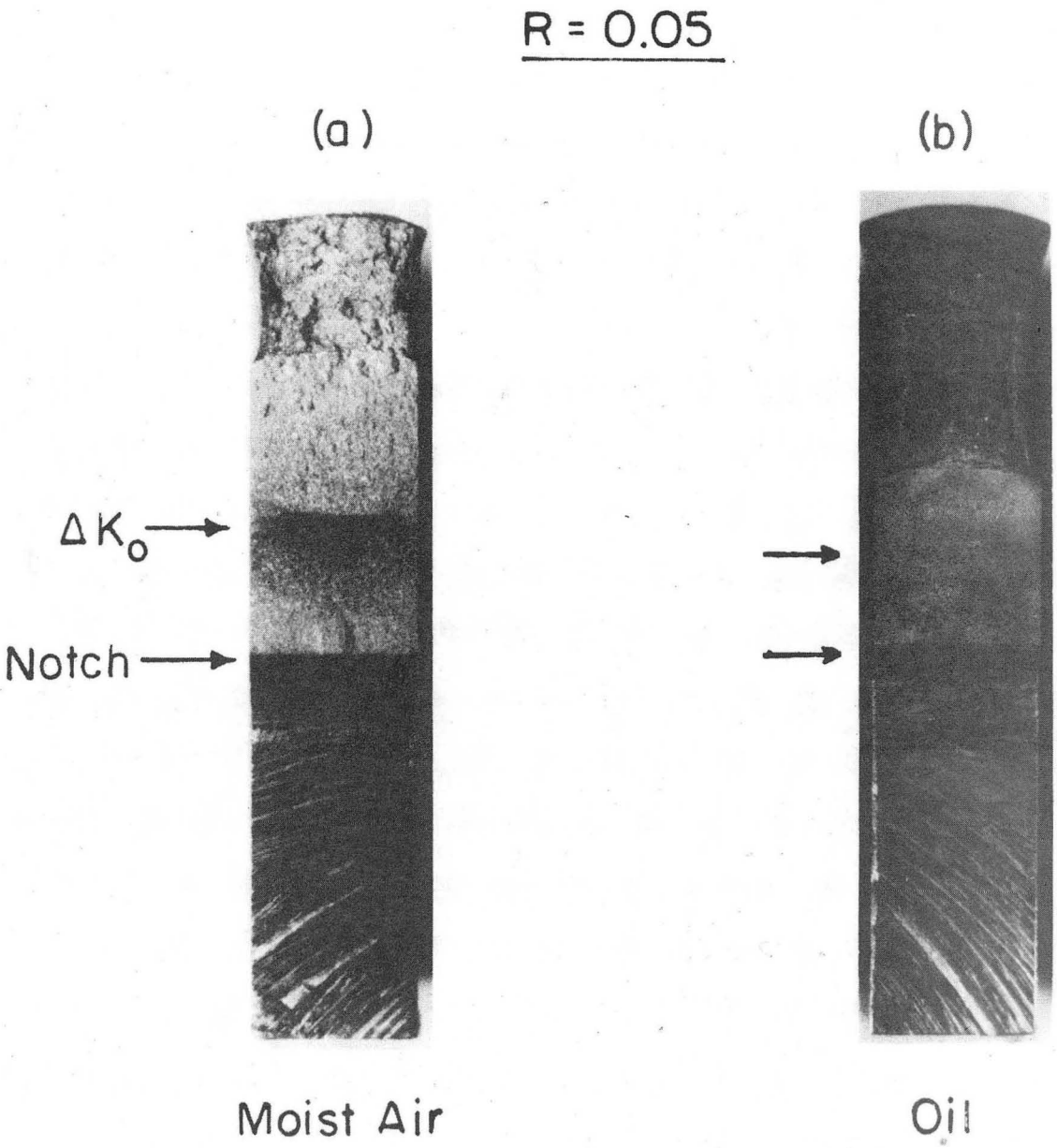

XBB 834-3827

Fig. 12. Typical macroscopic appearances of the fatigue fracture surfaces of SA542-3 steel tested in (a) moist air [32] and (b) oil environments at R = 0.05, showing the absence of oxide band on near-threshold fracture surfaces obtained in oil environments.

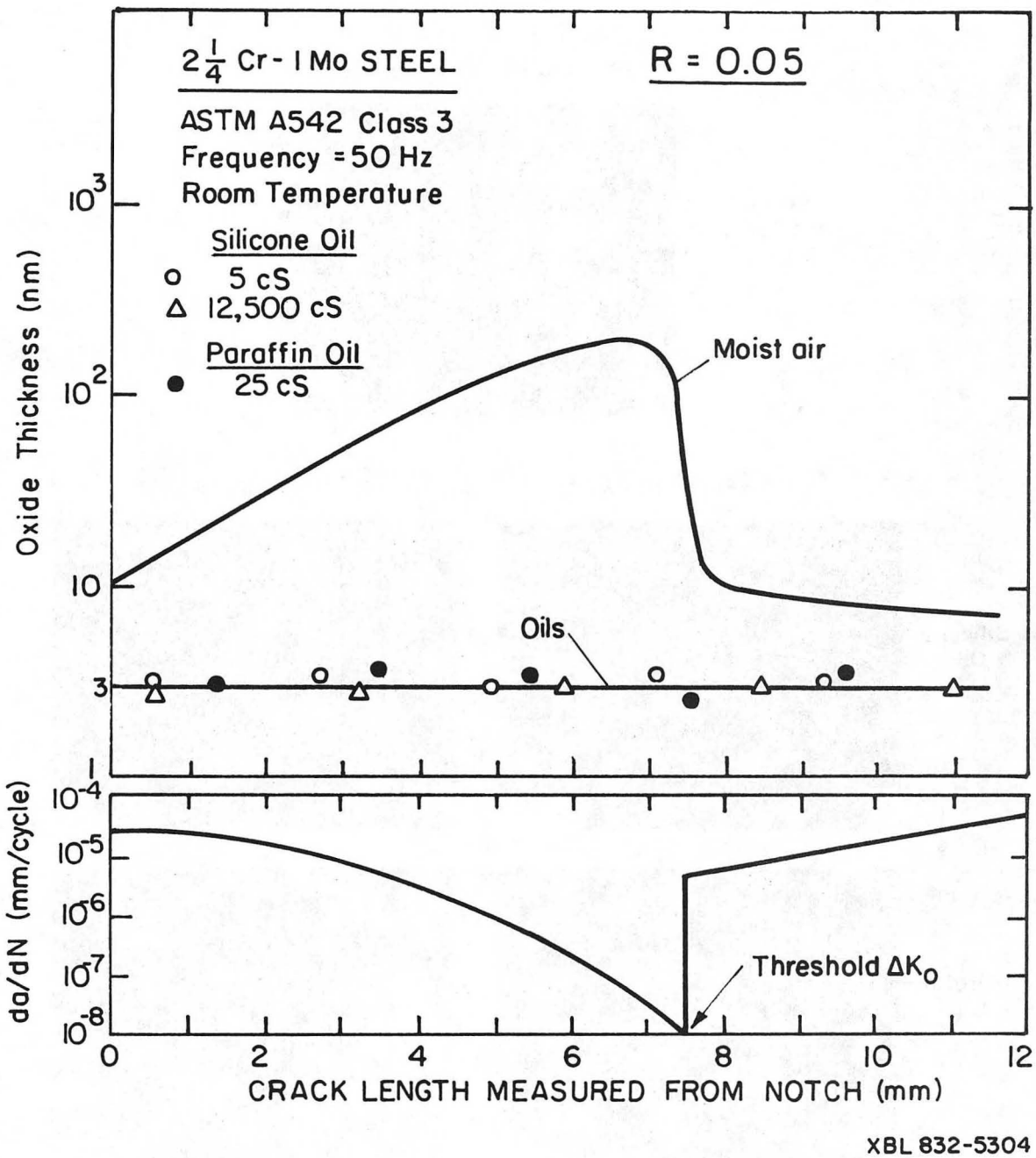

Fig. 13. Measurements of oxide thickness as a function of crack length measured from notch and crack growth rate (da/dN) for SA542-3 steel tested in oil environments (data points) and in moist air (data curve) [32]. Data from Ar^+ sputtering rate = 150 Å/min, sputtering time = 4 minutes).

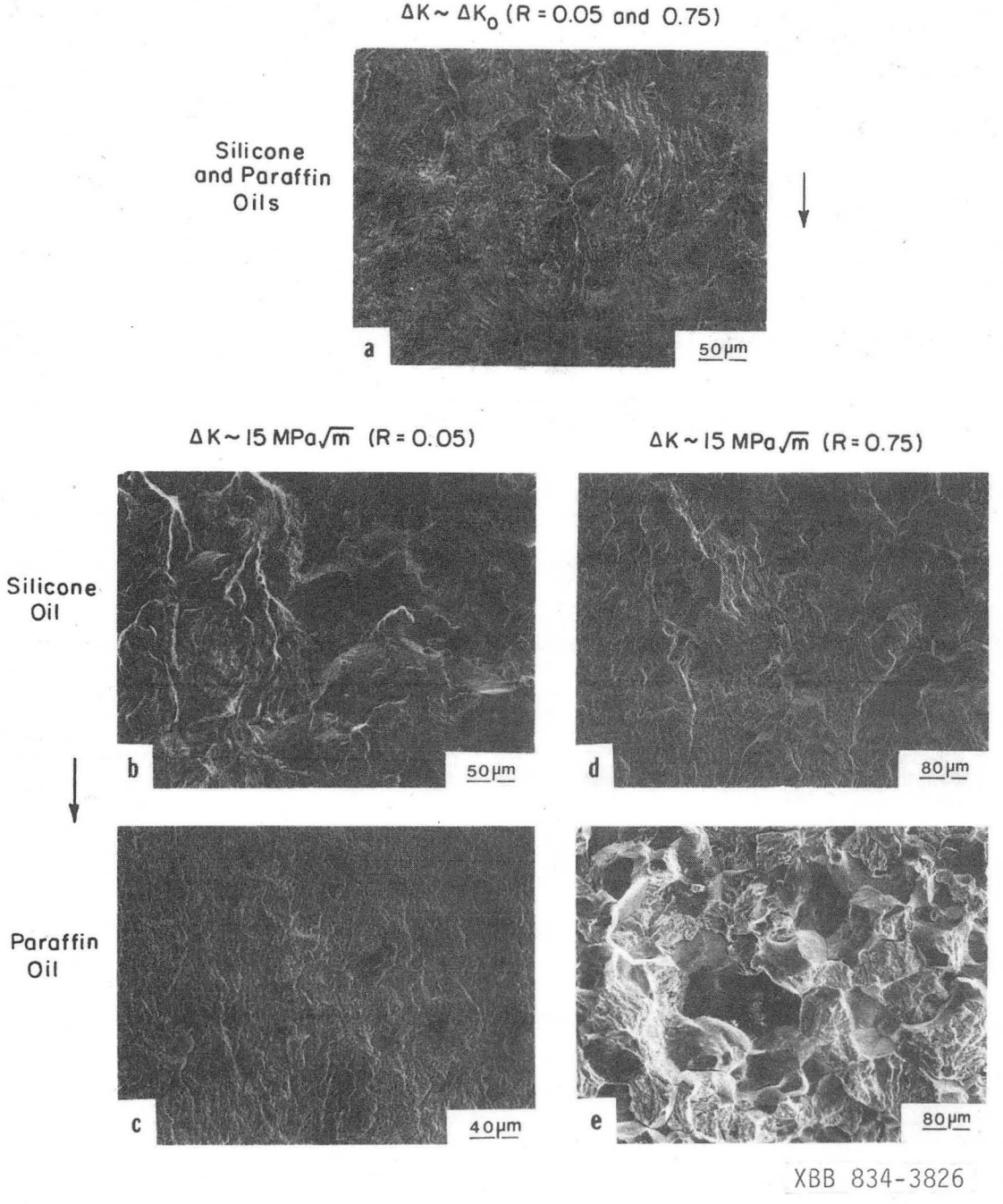

Fig. 14. Typical near-threshold ($\Delta K \sim \Delta K_0$) (a) and higher growth rate ($\Delta K \sim 15$ MPa$\sqrt{m}$) (b-e) fractography of fatigue crack growth in SA542-3 steel tested at R = 0.05 and 0.75 in silicone oils (a,b,d) and paraffin oils (a,c,e). Arrow indicates general direction of crack growth.

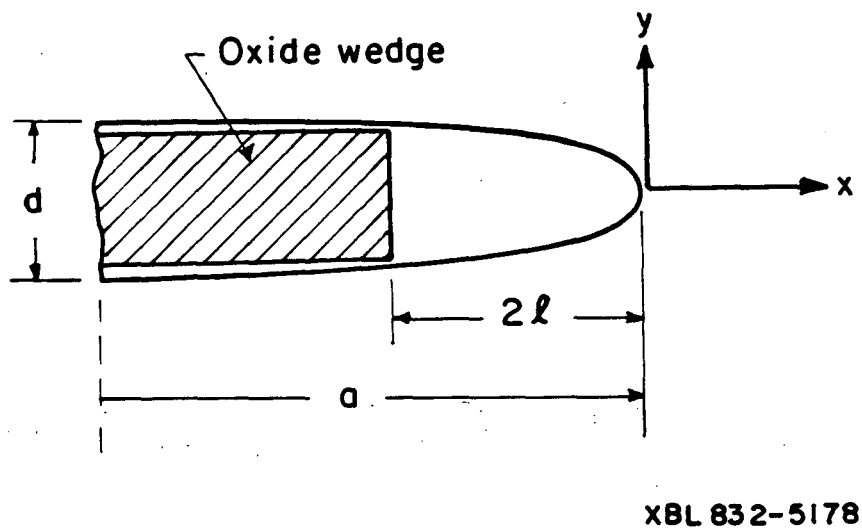

Fig. 15. Oxide-induced crack closure model for a near-threshold fatigue crack [34].

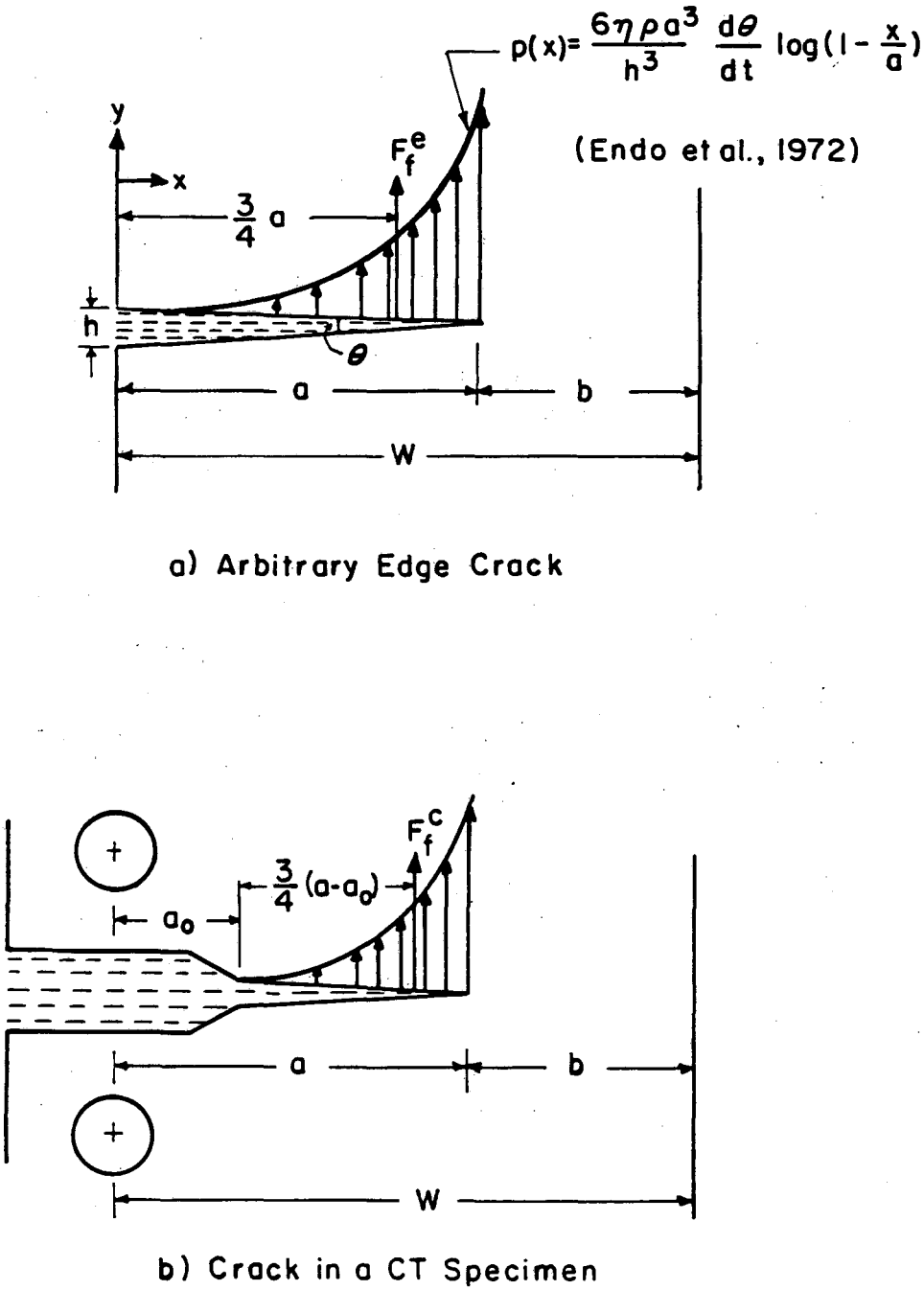

Fig. 16. Idealizations of the pressure distribution and the hydrodynamic action due to full penetration of viscous fluids into (a) an edge crack and (b) a crack in CT specimen, based on Endo et al. [5,6].

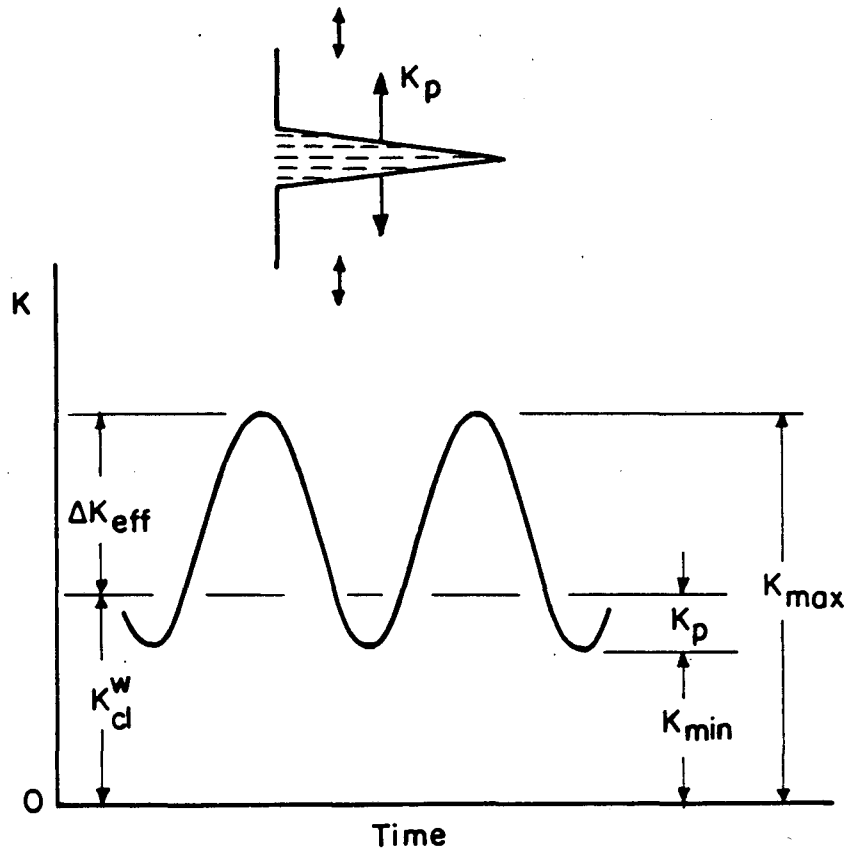

XBL 834-5538

Fig. 17. Schematic expressions for the crack closure effect due to hydrodynamic wedge action. K_p is the stress intensity increment due to hydrodynamic wedge when crack closes, raising the nominal K_{min} to K_{cl}^{w} and reducing the nominal ΔK (= K_{max} - K_{min}) to ΔK_{eff} (= K_{max} - K_{cl}^{w}).

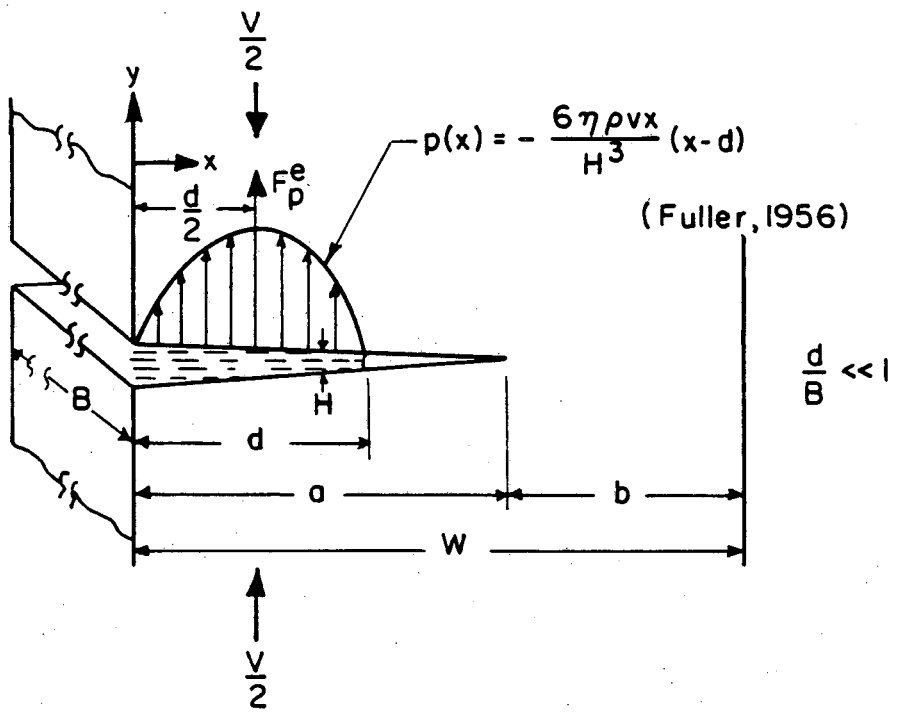

a) Arbitrary Edge Crack

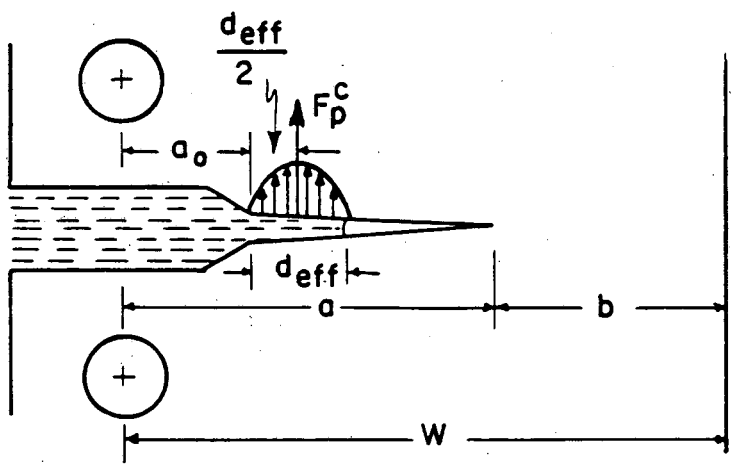

b) Crack in a CT Specimen

XBL834-5540

Fig. 18. Idealizations of the pressure distributions and the hydrodynamic wedge actions due to partial penetration of viscous fluids into (a) an edge crack and (b) a crack in CT specimen.

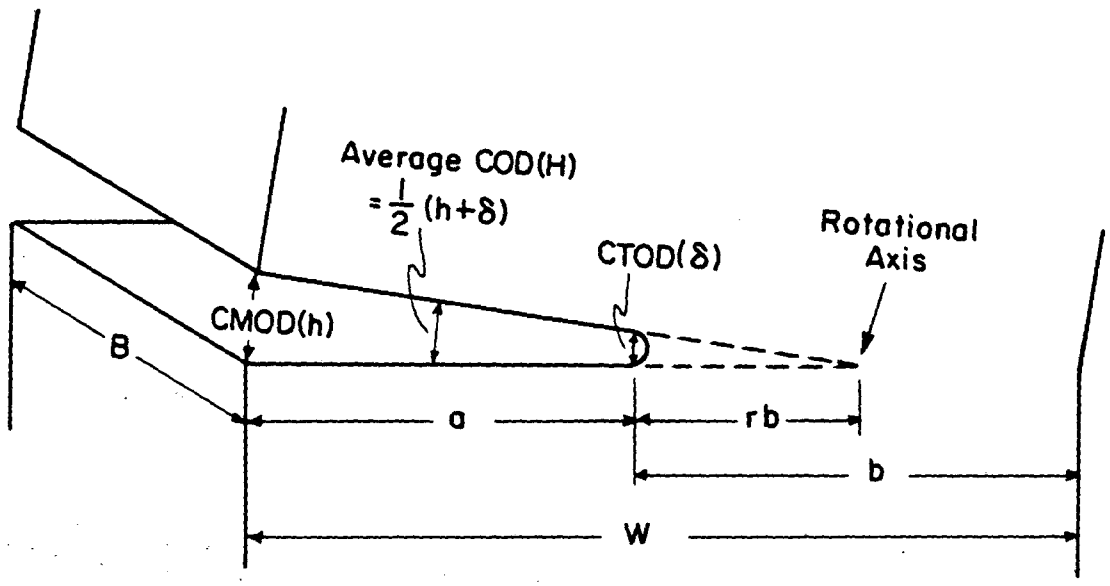

XBL 834-5539

Fig. 19. Idealized fatigue crack with a trapezoidal shape and a plastic hinge (or rotational axis) when subjected to cyclic loading.

This report was done with support from the Department of Energy. Any conclusions or opinions expressed in this report represent solely those of the author(s) and not necessarily those of The Regents of the University of California, the Lawrence Berkeley Laboratory or the Department of Energy.

Reference to a company or product name does not imply approval or recommendation of the product by the University of California or the U.S. Department of Energy to the exclusion of others that may be suitable.

TECHNICAL INFORMATION DEPARTMENT
LAWRENCE BERKELEY LABORATORY
UNIVERSITY OF CALIFORNIA
BERKELEY, CALIFORNIA 94720